atmosphere

MDPI

Article

Characteristics of Trace Metal Elements in Ambient Sub-Micron Particulate Matter in a Coastal Megacity of Northern China Influenced by Shipping Emissions from 2018 to 2022

Jinhua Du [1], Ziyang Liu [2], Wenxin Tao [1], Ting Wang [3], Jiaojiao Zhao [3], Weiwei Gong [4], Yue Li [4], Lian Xue [5], Jianli Yang [1], Chaolong Wang [1], Houyong Zhang [3], Fei Wang [6], Yingjie Sun [1] and Yisheng Zhang [1,*]

[1] School of Environmental and Municipal Engineering, Qingdao University of Technology, Qingdao 266520, China; dujinhua_1983@163.com (J.D.); taowx17860777652@163.com (W.T.); yjl17866827919@163.com (J.Y.); w15138755560@163.com (C.W.); sunyingjie@qut.edu.cn (Y.S.)

[2] Institute for Environmental and Climate Research, Jinan University, Guangzhou 511443, China; liuzy1997@stu2022.jnu.edu.cn

[3] Jinan Eco-Environment Monitoring Center of Shandong Province, Jinan 250100, China; wangting9105@163.com (T.W.); happyzhao_1988@163.com (J.Z.); sduzhy@163.com (H.Z.)

[4] Laboratory of Transport Pollution Control and Monitoring Technology, Transport Planning and Research Institute, Ministry of Transport, Beijing 100028, China; gongww@tpri.org.cn (W.G.); liyue@tpri.org.cn (Y.L.)

[5] Qingdao Eco-Environment Monitoring Center of Shandong Province, Qingdao 266003, China; xuelian710@163.com

[6] SunRui Marine Environment Engineering Co., Ltd., Qingdao 266071, China; wangfei@sunrui.net

* Correspondence: drzhang@live.cn

Abstract: Various shipping emission restrictions have recently been implemented locally and nationally, which might mitigate their impacts on regional air quality, climate change, and human health. In this study, the daily trace metal elements in PM_1 were measured in a coastal megacity in Northern China, from autumn to winter from 2018 to 2022, spanning DECA 1.0 (domestic emission control area), DECA 2.0, IMO 2020, and Pre-OWG Beijing 2022 stages. The trace element changes of V, Ni, Pb, and Zn in PM_1 were analyzed. The concentrations of V declined with shipping emission regulations implemented in 2018–2022 at 3.61 $\pm$ 3.01, 1.07 $\pm$ 1.04, 0.84 $\pm$ 0.62, and 0.68 $\pm$ 0.61 ng/m^3, respectively, with the V/Ni ratio decreasing at 1.14 $\pm$ 0.79, 0.93 $\pm$ 1.24, 0.35 $\pm$ 0.24, and 0.22 $\pm$ 0.18. The V/Ni ratio was dominated by the shipping emissions in the DECA 1.0 stage but has been more affected by the inland sources since DECA 2.0. The V/Ni ratio of local transport air mass was higher than that of long-distance transportation, indicating that some ships were still using high-sulfur fuel oil, especially for the ships 12 nautical miles from the coastline. The multiple linear regression model showed a better fit using V as a tracer for ship emission sources of ambient SO_2 in the DECA 1.0 stage, while the indication effect reduced since DECA 2.0. The V and V/Ni ratios should be carefully used as indicators of ship sources as more vessels will use clean fuels for energy, and the contribution of inland sources to V and Ni will gradually increase.

Keywords: vanadium; nickel; ship emission; PM_1; Qingdao

check for updates

Citation: Du, J.; Liu, Z.; Tao, W.; Wang, T.; Zhao, J.; Gong, W.; Li, Y.; Xue, L.; Yang, J.; Wang, C.; et al. Characteristics of Trace Metal Elements in Ambient Sub-Micron Particulate Matter in a Coastal Megacity of Northern China Influenced by Shipping Emissions from 2018 to 2022. *Atmosphere* **2024**, *15*, 264. https://doi.org/10.3390/atmos15030264

Academic Editors: Wei Tang, Cheol-Hee Kim and Fan Meng

Received: 31 December 2023
Revised: 3 February 2024
Accepted: 19 February 2024
Published: 22 February 2024

1. Introduction

Economic development brought about by growing ocean-going trade has negatively impacted urban climate, air quality, and human health [1–5]. SOx, NOx, OC, BC, and heavy metals released from the use of low-grade, high-sulfur fuels by marine vessels pose a serious threat to the atmospheric and marine environments, to the global climate, and to human health [1–3]. Particulate emissions from ships affect ocean chemistry and climate change [4], and their metal elements are stored in high concentrations in marine organisms, posing a risk of ingestion by humans and threatening human health [5,6]. In densely populated coastal areas with busy sea transportation, the pollutants emitted from ships impose a heavy burden on the quality of the atmospheric environment and human health [7]. Approximately 70% of ship emissions globally occur within 400 km of the coast, significantly impacting the air quality in and around ports, especially in densely populated urban areas [3,6]. Ship emissions within 12 nautical miles of the coast account for 51.2–56.5% of total ship emissions [7]. Affected by sea and land winds, the concentration of particulate matter in coastal cities increases by 4.7–38.1% on average due to ship emissions [8].

To reduce the impact of air pollution emissions from ships on the air quality of coastal cities, a series of policies have been introduced at home and abroad [9–16]. On 1 January 2016, the Ministry of Transport of China (MOT) determined the Beijing–Tianjin–Hebei region (BTH), the Yangtze River Delta (YRD), and the Pearl River Delta (PRD) as domestic emission control areas (DECA 1.0). It required ships berthed in the control areas to use 0.5% m/m of low-sulfur fuel [17]. On 1 January 2019, the domestic emission control area (DECA 2.0) expanded upon the DECA 1.0 policy, with the emission control area extending about 12 nautical miles along the entire coastline of the country and ships being required to use 0.5% (m/m) sulfur fuel for navigation and berthing [9,10]. On 1 January 2020, the International Maritime Organization (IMO) issued a regulation that the sulfur content of fuel oil used by ships in the global seas shall not exceed 0.5% m/m in the future (IMO 2020) [2] (Figures S1–S3). At the same time, before the 2022 Beijing Winter Olympics (October 2021–January 2022) (Pre-OWG Beijing 2022), the Ministry of Ecology and Environment implemented a series of policies to adjust the industrial, energy, and transportation structure in Tianjin, Hebei, and surrounding areas.

Studies have reported the impact of different ship emission control policies on air quality in coastal cities [17–19]. Observations conducted at Jingtang Port in Tangshan of northern China from December 2016 to January 2017 found that ambient SO_2 concentrations decreased rapidly since the DECA 1.0 policy was implemented on 1 January 2017 [20]. Observations at the Gaoqiao Port and Yangshan Port in Shanghai showed that, following the adoption of the DECA policy, the concentration of SO_2 reduction rate in port regions outpaced that in urban areas [21]. Compared with DECA 1.0 (2016–2019), the implementation of DECA 2.0 (2019–now) had a more significant effect on ship-source emission reduction [22,23].

V and Ni are high in emissions from ship fuel combustion and are often used as tracer elements [18,24–27]. The oceanic Ni and V cycling play essential roles in biogeochemical balance [28,29]. Ship emissions significantly contribute to V and Ni in most East Asian coastal areas, contributing more than 60% to V and 40% to Ni [22]. The observations at Chongming Island in Shanghai showed that the V concentrations in the DECA 2.0 stage significantly reduced between 2015 and 2019 compared with the DECA 1.0 stage. Implementation of DECA 2.0 resulted in a 60–70% reduction in V concentrations [22]. Based on the online monitoring data in port areas of Shanghai for four years (2017–2020), the concentration of V was reduced by 58%, and the concentration of Ni was decreased by 27% after the implementation of DECA 2.0. As the IMO 2020 policy was implemented, the V concentration decreased by 74%, and the Ni concentration decreased by 18% [30]. Liu et al. (2022) [31] observed PM_1 and its metal elements in Qingdao, showing that the V and Ni concentrations decreased by 73.3% and 22.1% in the DECA 2.0 stage compared with the DECA 1.0 stage. In addition to V and Ni, emissions of other heavy traces (Pb, Cd, As, and Zn) would be reduced accordingly [23].

The V/Ni ratio of direct emissions from heavy fuel oil combustion was much higher than those of the thermal power industry and chemical production [31–33]. Previous studies have reported the relationship between the dynamic changes in the V/Ni ratio and the impact of ship sources on air quality in inland and coastal sites [30]. Before the implementation of DECA 2.0, the V/Ni ratio in particulate matter in coastal cities such as Shanghai (more than 1.0) and Qingdao (more than 0.7) were higher than those of Zhengzhou (0.34), Xinxiang (0.22) and Taiyuan (0.43), Chengdu (0.41), and other inland cities [31,34–36]. However, current research needs more reports on the proportion of metal trace elements in the follow-up policy of DECA 2.0.

Particulate matter is still a major issue in North China in autumn/winter, while the sources of V and Ni in particulate matter in coastal cities are still unclear [31,37]. Qingdao is a crucial coastal megacity with a world-leading port in Northern China [31,38]. Even while facing the challenge of the COVID-19 pandemic, the foreign trade cargo throughput in the Port of Qingdao still steadily increased [39]. In this study, the trace metal elements in sub-micron particulate matter (PM_1) were measured in Qingdao in Northern China in the autumn/winter seasons for four consecutive years (2018–2022), spanning different shipping policy implementation stages (DECA 1.0, DECA 2.0, IMO 2020, and Pre-OWG Beijing 2022). The potential transport and spatial distribution of trace metal elements were analyzed using the airflow backward trajectory method. This study also provides further insights into the future air quality in coastal cities in eastern China under the increasingly stringent emission control from land and marine sources.

2. Materials and Methods

2.1. Sample Collection

2.1.1. Sampling Site and Time

The sampling site (36°05′ N, 120°21′ E) is located on the 7th-floor platform of Qingdao University of Technology (QUT) in Shibei District (71 m above sea level) (Figure 1). The improved six-channel ambient air particle sampler (ZR-3930 multi-channel type, ZhongRui, Inc., Qingdao, China) was used to collect PM_1 samples. One channel was for a 47 mm Teflon filter (Whatman, Marlborough, MA, USA), and another five channels were for quartz filters. The sampling time was in autumn and winter (November to January of the following year) (Table 1). The flow rate was 16.7 L/min. The daily sampling period was 09:30 to 08:30 of the next day. After sampling, the filter was stored at −18 °C.

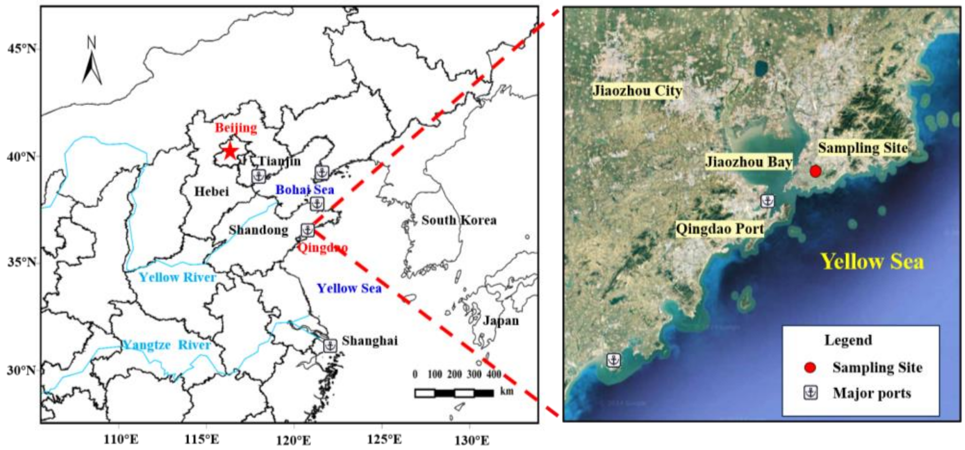

Figure 1. Location of the sampling site.

Table 1. The observation period under different shipping policies.

Shipping Policy Stage	Implementation Time	Observation Time	Number of Samples
DECA 1.0	1 January 2016–31 December 2018	1 November 2018–31 December 2018	61
DECA 2.0	Since 1 January 2019	1 January 2019–20 January 2019 1 November 2019–31 December 2019	80
IMO 2020	Since 1 January 2020	1 January 2020–20 January 2020 1 November 2020–31 December 2020 1 January 2021–20 January 2021	101
Pre-OWG Beijing 2022	October 2021–January 2022	1 November 2021–31 December 2021 1 January 2022–20 January 2022	81

2.1.2. Sample Analysis

The Teflon filter was equilibrated for 24 h (temperature: 20 ± 2 °C; relative humidity: 50 ± 5%) before and after sampling and then weighed (XPE-105, Mettler Toledo, Columbus, OH, USA). The detection and analysis process of metal elements in PM_1 includes Teflon filter pretreatment (digestion, acid removal, and constant volume) and instrument detection. The Teflon filter was cut and placed in the digestion tank, and 6 mL HNO_3 (GR) and 2 mL HF (GR) were added. A microwave digestion apparatus was used to heat to 190 °C for 25 min. Excess acid in the canister was evaporated in a fume hood and brought to a certain volume and fixed to 30 mL with ultrapure water. The concentrations of metal elements (Zn, Pb, Ni, V, and other trace metals) in PM_1 samples were determined by an inductively coupled plasma mass spectrometer (ICP-MS, PerkinElmer, Waltham, MA, USA).

2.1.3. Quality Assurance/Quality Control (QA/QC)

Before sampling, the quartz filter was baked in a muffle furnace at a temperature of 500 °C for 5.5 h. When analyzing the metal elements in the digestion solution, two blank filters were added to the same batch of filter samples to determine whether the samples were contaminated during the digestion and detection. Rhodium was used as the internal standard solution for ICP-MS analysis, and 1% HNO_3 was used to flush the pipeline before detection. In this study, the concentrations of the above metal elements were all within the detectable range, and the correlation coefficients of the standard curves were above 0.999. At the same time, every ten samples were tested and analyzed for quality control samples, and the standard error was required to be less than 5%. The background value of the blank sample was deducted.

2.2. Pollutant and Meteorological Data

The location of the national automatic air-monitoring substation was 618 m away from the sampling site. The hourly pollutant concentrations (PM_{10}, $PM_{2.5}$, CO, NO_2, SO_2, and O_3) in the site were obtained from the Qingdao Eco-environment Monitoring Center of Shandong Province. The hourly meteorological data (temperature (T), relative humidity (RH), wind direction (WD), and wind speed (WS)) were obtained from Fulongshan Meteorological Station (120°19′43′′ E, 36°04′20′′ N), 4.6 km away from the sampling site. The visibility (VIS) came from the Qingdao Liuting Airport Station (https://rp5.ru, accessed on 20 December 2023). The height of the planetary boundary layer (PBL) data were extracted from MeteoInfo 2.2.3.

2.3. Analysis Method

2.3.1. K-Means Clustering

The method assumes that the dataset X contains n data points with d-dimensional attributes, $X = \{x_1, x_2, \ldots x_n\}$, where $x_1 \in R^d$. K-means clustering aims to divide the n sample points into the specified K clusters according to the similarity of the samples between the datasets, and each sample only belongs to one of the clusters with the smallest distance from the center point. First, the K-means clustering algorithm randomly generates K cluster center points $C = \{c_1, c_2, \ldots c_k\}$, and then calculates the Euclidean distance from each data point to all cluster centers. The data points are assigned to the cluster center points with the smallest distance. Finally, the clustering effect is evaluated by calculating the sum of the squares of the distances between each data point and its cluster center points, even if the following function values are minimized:

$$\sum_{\substack{i=1 \\ j\in\{1,2,\ldots k\}}}^{n} min \left\|x_i - c_j\right\|^2 \tag{1}$$

This study performed K-means clustering based on V and Ni concentrations in the DECA 2.0 stage by software SPSS 26.

2.3.2. Enrichment Factor

The enrichment factor (EF) method was used to calculate the enrichment of trace elements in PM_1, which was used to determine whether the PM_1 fraction was more influenced by natural sources or anthropogenic sources [40,41]:

$$EF = (C_i / C_r) / (X_i / X_r) \quad (2)$$

where EF is the enrichment factor, C_i is the concentration of trace elements in PM_1, C_r is the concentration of reference trace elements in PM_1, X_i is the crustal abundance value of the measured trace elements, and X_r is the crustal abundance value of the reference trace elements. Al was selected as the reference factor for this study [42]. When the EF is less than 10, it indicates that the trace element is mainly influenced by natural sources from the earth's crust. When the EF is greater than 10, it suggests that the trace element is more influenced by anthropogenic sources [43,44].

2.3.3. Backward Trajectory and Clustering Analysis

The airflow backward trajectory is the air mass trajectory with a similar spatial distribution that arrives at the research site, and the TrajStat model is used for cluster analysis to explore the long-distance transport of atmospheric particles [31,45]. The MeteoInfo software was adopted with a start time of 8:00 am and corresponding daily PM_1 concentration. The backward pollution trajectory for 48 h was tracked.

2.3.4. Potential Source Contribution Factor Analysis

Potential source contribution function analysis (PSCF) is a conditional probability expressing the grid cell (divided into 0.5° × 0.5° latitude and longitude grids) that the pollutant concentration at the target location exceeds the standard threshold. This study set the 75th percentile of the sample as the potential contribution of a standard threshold [37,46], defined as

$$PSCF_{ij} = x_{ij} / y_{ij} \quad (3)$$

y_{ij} represents the total number of trajectories passing through a grid unit; x_{ij} is the number of trajectories exceeding the threshold standard in the same grid unit.

As PSCF is a probability value, the smaller the pollution trajectory value (y_{ij}), the easier it is to cause the PSCF value to fluctuate and increase the uncertainty of the PSCF value. Therefore, a weighting function W_{ij} is introduced to obtain the revised potential source contribution factor (WPSCF) to reduce the uncertainty of this value [45]:

$$WPSCF_{ij} = PSCF_{ij} \cdot W_{ij} \quad (4)$$

$$W_{ij} = \begin{cases} 1.00 & (80 < y_{ij}) \\ 0.72 & (20 < y_{ij} < 80) \\ 0.42 & (10 < y_{ij} < 20) \\ 0.05 & (y_{ij} < 10) \end{cases} \quad (5)$$

3. Results

3.1. Meteorological Parameters and Pollutant Concentrations

Under different shipping policies (DECA 1.0, DECA 2.0, IMO 2020, and Pre-OWG Beijing 2022), the prevailing wind direction was northwest but the area was also affected by easterly and southeasterly winds (Figure 2). The wind speeds under different policies were 3.29 ± 1.68, 3.60 ± 1.53, 3.52 ± 1.54, and 3.44 ± 1.58 m/s, respectively (Table 2; Figure S4). The relative humidity differences were minor from DECA 1.0 to Pre-OWG Beijing 2022 stages, which were 63.7 ± 11.5%, 62.9 ± 14.5%, 60.1 ± 14.6%, and 59.2 ± 14.6%, respectively. Compared with the DECA 1.0 stage, the VIS in the Pre-OWG Beijing 2022 stage was improved by 15.2% (DECA 1.0: 13.2 ± 8.08 km, DECA 2.0: 13.83 ± 8.65 km, IMO 2020: 15.2 ± 8.49 km, Pre-OWG Beijing 2022: 15.9 ± 9.0 km).

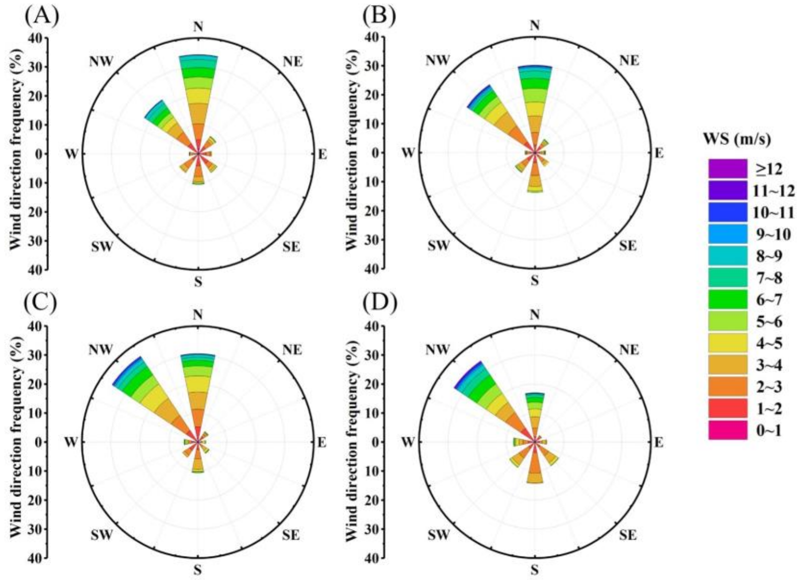

Figure 2. Wind rose diagram in DECA 1.0 (**A**), DECA 2.0 (**B**), IMO 2020 (**C**), and Pre-OWG Beijing 2022 (**D**).

Table 2. Meteorological conditions and concentrations of gaseous pollutants and particulate matter during observation period.

Types	DECA 1.0 (*n* = 61)		DECA 2.0 (*n* = 80)		IMO 2020 (*n* = 101)		Pre-OWG Beijing 2022 (*n* = 81)	
	Range	Average	Range	Average	Range	Average	Range	Average
T (°C)	−6.22–16.1	6.50 ± 6.04	−3.79–17.5	5.60 ± 5.60	−10.9–17.3	3.98 ± 5.96	−7.10–17.8	6.24 ± 5.55
VIS [1] (km)	1.03–29.6	13.2 ± 8.08	0.74–28.6	13.8 ± 8.65	1.88–30.0	15.2 ± 8.49	1.50–30.0	15.9 ± 8.98
WS (m/s)	1.13–7.93	3.29 ± 1.68	1.39–7.96	3.60 ± 1.53	1.17–8.77	3.52 ± 1.54	1.28–8.43	3.44 ± 1.58
RH (%)	39.8–93.9	63.7 ± 11.5	29.3–97.3	62.9 ± 14.5	36.4–91.8	60.1 ± 14.6	27.5–91.2	59.2 ± 14.6
SO_2 (μg/m^3)	2.96–34.9	12.4 ± 7.03	4.00–31.2	13.4 ± 6.08	5.00–39.4	15.1 ± 6.71	4.23–22.0	9.68 ± 3.41
NO_2 (μg/m^3)	21.8–118	55.8 ± 21.6	14.2–106	58.2 ± 21.8	5.62–115	47.4 ± 20.6	11.8–84.5	45.8 ± 18.2
PM_{10} (μg/m^3)	30.3–493	114 ± 78.7	18.6–375	109 ± 64.4	25.0–325	96.0 ± 59.4	14.5–205	77.5 ± 44.3
$PM_{2.5}$ (μg/m^3)	12.5–186	59.4 ± 41.4	10.6–286	67.1 ± 54.8	7.86–257	60.8 ± 49.2	8.04–161	47.3 ± 32.5

[1] VIS represents visibility.

The PM_1 concentrations during DECA 1.0, DECA 2.0, IMO 2020, and Pre-OWG Beijing 2022 were 37.9 ± 22.2, 42.2 ± 29.3, 41.9 ± 28.8, and 34.3 ± 22.4 μg/m^3, respectively (Table 3; Figure S5). Among different policies, the observed results in Qingdao were higher than those in coastal cities at home and abroad (Tianjin: 32.4 μg/m^3, Venice: 26.2 μg/m^3, Bologna: 15.5 μg/m^3 and Salento Peninsula: 15 μg/m^3) [47–50]. But they were lower than that of Xi'an (178.2 μg/m^3) [51], Wuhan (117.2 μg/m^3) [52], and Beijing (78.2 μg/m^3) [45].

Compared with the IMO 2020 stage, the PM_1, $PM_{2.5}$, and PM_{10} decreased by 18.1%, 22.2%, and 19.5% in the Pre-OWG Beijing 2022 stage, respectively. The results showed that the emission reduction policy before the Winter Olympics also played a crucial role in reducing the concentration of atmospheric particulate matter in Qingdao. Under the DECA 1.0, DECA 2.0, and IMO 2020 stages, the SO_2 concentration (12.4 ± 7.03, 13.4 ± 6.08, and 15.1 ± 6.71 μg/m^3) slightly increased. During the Pre-OWG Beijing 2022 stage, the SO_2 concentration decreased significantly, with a decrease of 35.9% compared with the IMO 2020 stage.

Table 3. V, Ni, Zn, and Pb in PM_1 and their ratios under different policies.

Types	DECA 1.0		DECA 2.0		IMO 2020		Pre-OWG Beijing 2022	
	Range	Mean ± SD	Range	Mean ± SD	Range	Mean ± SD	Range	Mean ± SD
PM_1 (μg/m³)	9.36–108	37.9 ± 22.2	7.74–123	42.2 ± 29.3	6.29–154	41.9 ± 28.8	4.99–95.8	34.3 ± 22.4
V (ng/m³)	0.03–11.1	3.45 ± 3.01	0.19–5.39	1.07 ± 1.04	0.00–3.02	0.84 ± 0.62	0.00–3.27	0.68 ± 0.61
Ni (ng/m³)	0.25–10.9	2.86 ± 2.27	0.11–5.83	1.90 ± 1.20	0.71–15.6	2.90 ± 2.41	0.21–13.8	3.57 ± 2.43
Zn (ng/m³)	12.32–298	64.4 ± 50.8	3.75–262	59.6 ± 49.9	3.26–193	64.6 ± 38.4	6.31–323	65.3 ± 46.8
Pb (ng/m³)	3.92–60.7	19.8 ± 13.4	0.96–54.8	16.0 ± 12.3	2.38–68.0	21.0 ± 11.7	2.15–34.8	12.7 ± 6.54
V/Ni	0.05–2.98	1.14 ± 0.79	0.10–7.65	0.93 ± 1.24	0.00–1.43	0.35 ± 0.24	0.00–0.95	0.22 ± 0.18
V/Zn	0.00–0.48	0.07 ± 0.09	0.00–0.48	0.05 ± 0.10	0.00–0.70	0.03 ± 0.08	0.00–0.17	0.02 ± 0.03
V/Pb	0.00–0.90	0.20 ± 0.20	0.01–1.77	0.17 ± 0.35	0.00–0.96	0.07 ± 0.12	0.00–0.50	0.07 ± 0.08

Emissions from burning crude oil as energy for ships contain V, Ni, Zn, and Pb, which were used as tracers of ship sources [37,53–56]. The V concentrations during DECA 1.0, DECA 2.0, IMO 2020, and Pre-OWG Beijing 2022 were 3.61 ± 3.01, 1.07 ± 1.04, 0.84 ± 0.62, and 0.68 ± 0.61 ng/m^3, respectively (Figure 3). In both the DECA 1.0 and DECA 2.0 stages, the V concentrations in PM_1 were lower than the observation results in Shanghai (10.98 and 9.44 ng/m^3) [30], which was related to the higher number of ships in Shanghai Port than in Qingdao Port. Compared with the DECA 1.0 stage, V dropped by 70.3% in the DECA 2.0 stage, 73.4% in the IMO 2020 stage, and 80.3% in the Pre-OWG Beijing 2022. The Ni, Zn, and Pb in the DECA 2.0 stage decreased by 33.6%, 7.45%, and 19.2%, respectively. Compared with the DECA 2.0 stage, the Ni, Zn, and Pb in the IMO 2020 stage had increased by 52.6%, 8.39%, and 31.2%, respectively. With the changes in the policy, the concentration of V had decreased significantly. Ni, Pb, and Zn had no significant changes, indicating other potential sources.

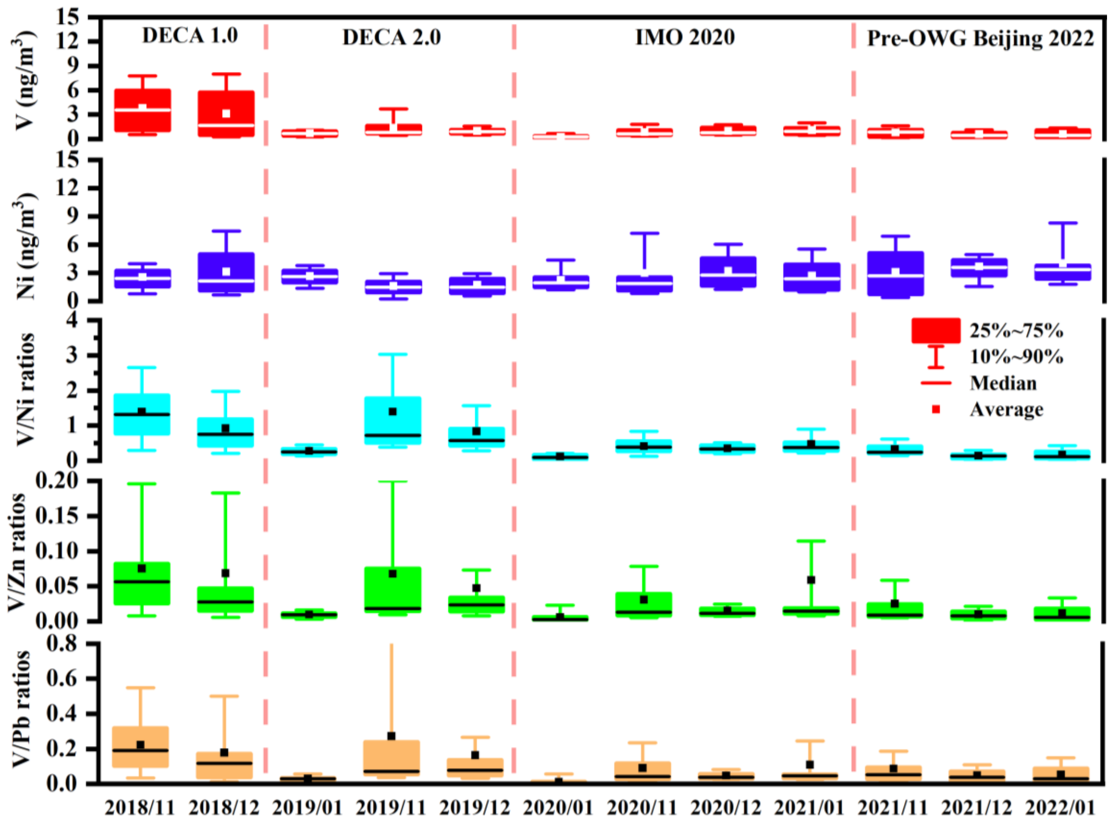

Figure 3. Monthly concentrations of V and Ni in PM_1 under different shipping policies.

Previous studies have shown that using low-sulfur fuel in ships reduces the concentration of V-containing pollutants [20,57]. Changes from heavy fuel to low-sulfur fuel reduce the concentration of V in the atmosphere [20,31]. The DECA 2.0 policy significantly reduced ship emissions in Qingdao and had similar effect compared with the IMO 2020 stage. On the other hand, the fuel oil used by ships in 2019 and 2020 was mainly heavy oil, light oil, or diesel/gasoline, accounting for 95.03% and 94.01%, respectively [58,59]. Compared with 2019, the use of LNG in 2020 increased by 14.23%. From January 2018 to May 2022, the cargo throughput of Qingdao Port showed an overall growth trend, indicating that the number of ships under different shipping policies increased slowly (Figure S6). From 2016 to 2022, the operation of LNG-fueled vessels and the number of planned equipment increased dramatically on a yearly basis (Figure S7). Consistent with the conclusions obtained from the field experiment in the Pearl River Delta [60], V should be carefully considered as a tracer element for ship sources as more vessels will use clean fuels for energy in the future.

3.2. Source Analysis Based on the Ratio Method

The V/Ni, V/Zn, and V/Pb ratios can be used to identify ship emission sources [31,56,61]. When the V/Ni, V/Zn, and V/Pb were less than 0.7, 0.11, and 0.09, the regional ship emission sources had less impact on the regional ambient air [56]. The V/Ni ratios in this research study were 1.14 $\pm$ 0.79, 0.93 $\pm$ 1.24, 0.35 $\pm$ 0.24, and 0.22 $\pm$ 0.18 during DECA 1.0, DECA 2.0, IMO 2020 and Pre-OWG Beijing 2022. Compared with the DECA 1.0 stage, the V/Ni ratio dropped by 18.4%, 69.3%, and 80.7% in the DECA 2.0, IMO 2020, and Pre-OWG Beijing 2022 stages. The V/Ni ratio in the DECA 2.0 stage ranged from 0.10 to 7.65, and there is still a high value (Figure 3). The V/Zn and V/Pb ratios were 0.07 $\pm$ 0.09 and 0.20 $\pm$ 0.20 in the DECA 1.0 stage, higher than those in Shijiazhuang (0.02 and 0.05) [62], Beijing (0.01 and 0.06) [63], Baoding (0.02 and 0.05) [62], and Langfang (0.02 and 0.02) [64]. The V/Zn and V/Pb ratios decreased by 28.6% and 5% in DECA 2.0, 57.1% and 65.0% in IMO 2020, and 71.4% and 65.0% in the Pre-OWG Beijing 2022 stage. After implementing the IMO 2020 policy, the V/Ni, V/Zn, and V/Pb ratios stabilized at a smaller value.

The V/Pb ratios of DECA 1.0, DECA 2.0, IMO 2020, and Pre-OWG Beijing 2022 were 0.20 $\pm$ 0.20, 0.19 $\pm$ 0.37, 0.07 $\pm$ 0.12, and 0.02 $\pm$ 0.03 ng/m^3, respectively. The V/Pb ratios in the DECA 1.0 and DECA 2.0 stages were higher than those observed by [32] (0.11–0.27 ng/m^3, $PM_{2.5}$). Compared with the IMO 2020 stage, the Pre-OWG Beijing 2022 stage dropped by 71.4% due to the stringent control and emission reduction in industrial enterprises in BTH and surrounding cities during the preparatory stage for the Winter Olympics.

The correlation coefficients R2 of V and Ni were 0.48, 0.01, 0.18, and 0.32 in DECA 1.0, DECA 2.0, IMO 2020, and Pre-OWG Beijing 2022, respectively. Since the implementation of DECA 2.0, the primary sources of V and Ni have changed considerably [23,31]. Based on domestic and foreign research, the V/Ni ratios of domestic and foreign coastal sites are summarized in Tables 4–6. The V/Ni ratios of particulate matter in coastal cities were similar to the slope of the regression line in the DECA 1.0 stage (Figure 4). After the implementation of DECA 2.0, the V/Ni ratios in inland sites were similar to the slopes of DECA 2.0, IMO 2020, and Pre-OWG Beijing 2022. Since the implementation of DECA 2.0, the V/Ni ratio has decreased due to the steady decline in ship emission sources and it was gradually influenced by inland coal-burning and motor vehicle sources.

K-means clustering of V and Ni concentrations could classify the data in the DECA 2.0 stage into three classes (Type I, Type II, and Type III) (Figure 5). The V/Ni ratios of different linearity were 0.49 $\pm$ 0.27, 1.28 $\pm$ 0.94, and 5.52 $\pm$ 1.90, respectively. This indicated that the DECA 2.0 stage belonged to the transition stage of the DECA 1.0 and the IMO 2020. The linear slope of Type I was 0.11, which was similar to the linear slope of the IMO 2020 and Pre-OWG Beijing 2022 stages. The dominant wind directions of Type I were northerly (wind direction frequency: 36%) and northwesterly (wind direction frequency: 30%), which were less affected by the discharge from ships (Figure 6). The linear slope of Type II (2.06) was much higher than that in DECA 1.0, indicating dominance by ship emissions. The dominant wind direction in Type II was south (frequency of 35%), further suggesting the impact of ship emissions. This further verified that a number of ships still used heavy fuel oil outside the emission control area in the DECA 2.0 stage. The oceanic transport air mass arrived in Qingdao, increasing the V/Ni ratio in the region [61]. The dominant wind direction in Type III was northwesterly, with wind speed of 3.89 ± 2.49 m/s and PBL of 520 ± 293 m. V and Ni concentrations ranged from 0.83 to 1.69 ng/m3 and 0.11 to 0.42 ng/m^3, respectively. The V and Ni concentrations were lower than DECA 2.0, but the Ni concentration decreased more. The inland emission reduction policy also impacted the V/Ni ratio and resulted in a high V/Ni ratio [31]. After the implementation of DECA 2.0, the V/Ni ratio should be carefully considered as an indicator for identifying regional pollution from ship sources.

Table 4. Trace elements and their ratios in particulate matter in coastal cities of China (Unit: ng/m^3).

Observation Time		Location	Particle Size	V	Ni	Zn	Pb	V/Ni	V/Zn	V/Pb	References
Before DECA 1.0	October 2014–September 2005	Hong Kong	PM_1	16	5.2	210	47	3.08	0.08	0.34	[65]
	March 2006–February 2007	Qingdao	$PM_{2.5}$	10	6	271	128	1.67	0.04	0.08	[44]
	January 2012–December 2012	Yantai	$PM_{2.5}$	6	4	94.3	91.7	1.50	0.06	0.07	[56]
	September 2013–August 2014	Ningbo	$PM_{2.5}$	7.36	8.25	190	56.3	0.89	0.04	0.13	[34]
	September 2013–August 2014	Shanghai	$PM_{2.5}$	16.5	14.9	215	69.7	1.11	0.08	0.24	[34]
	January 2015–December 2015	Tianjin	$PM_{2.5}$	17.1	10.8	80.5	19.8	1.58	0.21	0.86	[66]
DECA 1.0	January 2016–December 2016	Tangshan	$PM_{2.5}$	5.6	7.1	186	183	0.79	0.03	0.03	[67]
	January 2017–December 2017	Shanghai	$PM_{2.5}$	10.98	5.33	/	/	2.06	/	/	[30]
	January 2018–December 2018	Shanghai	$PM_{2.5}$	9.44	5	/	/	1.89	/	/	[30]
	January 2017–December 2017	Tangshan	$PM_{2.5}$	3.2	4.6	198	146	0.70	0.02	0.02	[67]
	January 2018–December 2018	Shenzhen	$PM_{2.5}$	11.6	4.76	/	31	2.44		0.37	[35]
	May 2018–July 2018	Tianjin	$PM_{2.5}$	2.2	12.1	86	19.4	0.18	0.03	0.11	[47]
	August 2018–May 2019	Qingdao	$PM_{2.5}$	10.68	22.88	130	355.2	0.47	0.08	0.03	[37]
DECA 2.0	January 2019–December 2019	Shanghai	$PM_{2.5}$	4.6	3.87	/	/	1.19	/	/	[30]
	January 2018–December 2019	Shanghai	$PM_{2.5}$	9.57	9.57	31.2	8.64	1	0.31	1.11	[68]
	August 2019	Tangshan	$PM_{2.5}$	2.3	1.53	41.6	14.2	1.5	0.06	0.16	[62]
IMO 2020	January 2020–December 2020	Shanghai	$PM_{2.5}$	1.19	3.18	/	/	0.37	/	/	[30]

Observation time of this research spanned from DECA 1.0 to DECA 2.0.

Table 5. Trace elements and their ratios in particulate matter in Chinese inland cities (Unit: ng/m^3).

	Observation Time	Location	Particle Size	V	Ni	Zn	Pb	V/Ni	V/Zn	V/Pb	References
Before DECA 1.0	March 2006–February 2007	Zibo	$PM_{2.5}$	8.23	10.55	1070	1630	0.78	0.01	0.01	[69]
	November 2011	Chengdu	$PM_{2.5}$	1.7	2.5	350	172	0.5	0	0.01	[70]
	September 2013–August 2014	Nanjing	$PM_{2.5}$	9.88	9.3	247	90.9	1.06	0.04	0.11	[34]
	September 2013–August 2014	Hangzhou	$PM_{2.5}$	15.3	10.4	495	122	1.47	0.03	0.13	[34]
	April 2013–June 2013	Beijing	$PM_{2.5}$	3.1	2.6	117	90	1.19	0.03	0.03	[51]
	December 2014–February 2015	Baoding	$PM_{2.5}$	10	40	1170	460	0.25	0.01	0.02	[71]
	March 2014–June 2015	Langfang	$PM_{2.5}$	10	40	330	140	0.25	0.03	0.07	[71]
DECA 1.0	October 2016–November 2016	Shijiazhuang	$PM_{2.5}$	8.85	17.7	398	185	0.5	0.02	0.05	[62]
	January 2016–December 2016	Beijing	$PM_{2.5}$	3.22	3.01	291	53.6	1.07	0.01	0.06	[63]
	September 2016–November 2016	Baoding	$PM_{2.5}$	8.85	17.7	398	185	0.5	0.02	0.05	[62]
	September 2016–January 2017	Baoding	$PM_{2.5}$	1.8	6.2	340	192	0.29	0.01	0.01	[64]
	September 2016–January 2017	Shijiazhuang	$PM_{2.5}$	2.8	6.1	288	124	0.46	0.01	0.02	[64]
	September 2016–January 2017	Langfang	$PM_{2.5}$	3.6	5.8	228	150	0.62	0.02	0.02	[64]
	January 2016–December 2017	Chengdu	$PM_{2.5}$	1.24	3.06	357	87.2	0.41	0	0.01	[36]
	January 2016–December 2017	Nanjing	$PM_{2.5}$	6.05	3.62	199	50.8	1.67	0.03	0.12	[72]
	January 2017	Shijiazhuang	$PM_{2.5}$	1.1	14.2	212	51.2	0.08	0.01	0.02	[73]
	September 2017–January 2018	Baoding	$PM_{2.5}$	1.2	4.4	188	80	0.27	0.01	0.02	[64]
	September 2017–January 2018	Langfang	$PM_{2.5}$	2.1	4.8	123	56	0.44	0.02	0.04	[64]
	October 2017–January 2018	Langfang	$PM_{2.5}$	4	6	198	68	0.67	0.02	0.06	[74]
	September 2017–January 2018	Shijiazhuang	$PM_{2.5}$	1.5	4.9	161	59	0.31	0.01	0.03	[64]
	June 2018	Shijiazhuang	$PM_{2.5}$	1.7	1.26	114	63.8	1.35	0.01	0.03	[75]
	July 2018	Shijiazhuang	$PM_{2.5}$	0.25	1.1	115	32.6	0.23	0	0.01	[75]
	November 2018–December 2018	Baoding	$PM_{2.5}$	0.51	3.12	979	279	0.16	0	0	[75]
	January 2018–December 2018	Taiyuan	$PM_{2.5}$	4.46	10.4	/	63.3	0.43	/	0.07	[35]
DECA 2.0	October 2018–January 2019	Shijiazhuang	$PM_{2.5}$	1.2	8	183	51	0.15	0.01	0.02	[76]
	December 2018–January 2019	Langfang	$PM_{2.5}$	0.16	2.2	184	67.5	0.07	0	0	[75]
	January 2019	Baoding	$PM_{2.5}$	0.7	1.44	123	38	0.49	0.01	0.02	[75]
	March 2019	Baoding	$PM_{2.5}$	4.66	2.96	698	156	1.57	0.01	0.03	[75]

Table 6. Trace elements and their ratio in particulate matter in inland and coastal cities abroad (Unit: ng/m^3).

Location	Country	Observation Time	Particle Size	V	Ni	Zn	Pb	V/Ni	V/Zn	V/Pb	References
Salento Island	Italy	July 2008–May 2010	PM_1	3	3	/	4	1	0.75	3.00	[50]
Venice	Italy	November 2010–July 2011	PM_1	8.0	1.7	22.1	/	4.7	/	1.70	[77]
Venice	Italy	December 2013–February 2014	PM_1	2.4	2.5	28	7	0.96	0.34	2.50	[48]
Salento Island	Italy	July 2008–May 2010	$PM_{2.5}$	4	5	/	7	0.80	0.57	5.00	[50]
Venice	Italy	January 2011–December 2011	$PM_{2.5}$	7	4	81	12	1.75	0.58	4.00	[78]
Genoa	Italy	January 2011–December 2011	$PM_{2.5}$	14	7	19	6	2.00	2.33	7.00	[78]
Barcelona	Spain	January 2011–December 2011	$PM_{2.5}$	6	3	42	6	2.00	1.00	3.00	[68]
Marseille	France	January 2011–December 2012	$PM_{2.5}$	6	4	24	8	1.50	0.75	4.00	[78]
Busan	South Korea	January 2013–December 2013	$PM_{2.5}$	8.3	4.4	92	30	1.89	0.28	4.39	[53]
Sao Paulo	Brazil	January 2014–December 2015	$PM_{2.5}$	2	17	320	44	0.12	0.05	16.67	[79]
Hayashizaki	Japan	January 2016–December 2017	$PM_{2.5}$	8.96	3.12	25.3	6.98	2.89	1.28	/	[80]
Tarumi	Japan	January 2016–December 2017	$PM_{2.5}$	10.2	3.35	22.5	7.61	3.04	1.34	3.36	[80]
Suma	Japan	January 2016–December 2017	$PM_{2.5}$	8.34	2.7	14.3	4.77	3.09	1.75	2.70	[80]
Estarreja	Portugal	September 2019–November 2019	$PM_{2.5}$	2.13	0.534	3.99	21.2	3.78	0.10	0.56	[81]
Frankfurt	Germany	June 2009–November 2010	PM_1	1.2	2.2	/	4.8	0.54	0.25	2.22	[82]
Tehran	Iran	May 2012–May 2013	PM_1	3.04	4.1	84.4	54.46	0.74	0.06	4.11	[83]
Frankfurt	Germany	June 2009–November 2010	$PM_{2.5}$	2.5	5.0	/	13	0.5	0.19	5.00	[82]
London	UK	January 2012–December 2012	$PM_{2.5}$	1.3	0.5	8.9	2.3	2.60	0.57	0.50	[84]
Tehran	Iran	May 2012–May 2013	$PM_{2.5}$	4.19	4.91	133.97	72.65	0.85	0.06	4.93	[83]
Makkah	Saudi Arabia	January 2012–December 2014	$PM_{2.5}$	3.2	20	19	15	0.16	0.21	20.00	[85]

Based on the results of EFs, the uncertainty of the V, Ni, and V/Ni ratio in ship source traceability after implementing the DECA 2.0 policy was further confirmed as the ship source traceability standard. Pb and Zn had EFs above 500 under different policies, indicating the influence of anthropogenic sources (Figure 7). In the DECA 1.0, DECA 2.0, IMO 2020, and Pre-OWG Beijing 2022 stages, the EFs of V were 30.0, 32.6, 8.46, and 4.18; the EFs of Ni were 45.0, 71.2, 41.2, and 32.7, respectively. Before the IMO 2020 stage, V and Ni were more affected by anthropogenic sources, consistent with the results in Jingtang Port in Tangshan [20]. Compared with the DECA 1.0 stage, the V concentration in the Pre-OWG Beijing 2022 stage decreased by 86.1%. After the implementation of IMO 2020, the source of V was affected by both anthropogenic and natural sources.

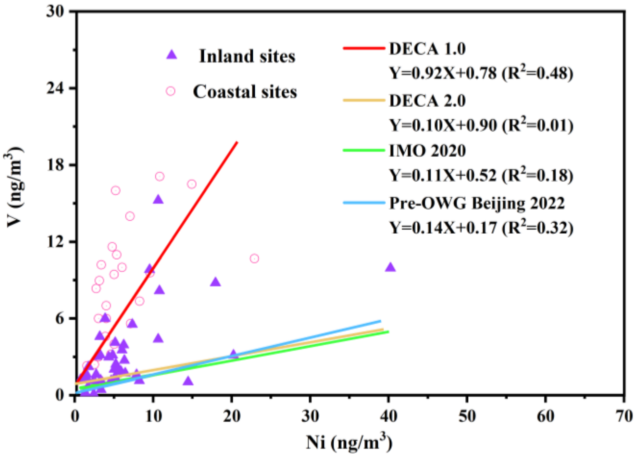

Figure 4. Linear regression between V and Ni at observation site under different shipping policies. Points are literature-reported V and Ni in inland and coastal sites.

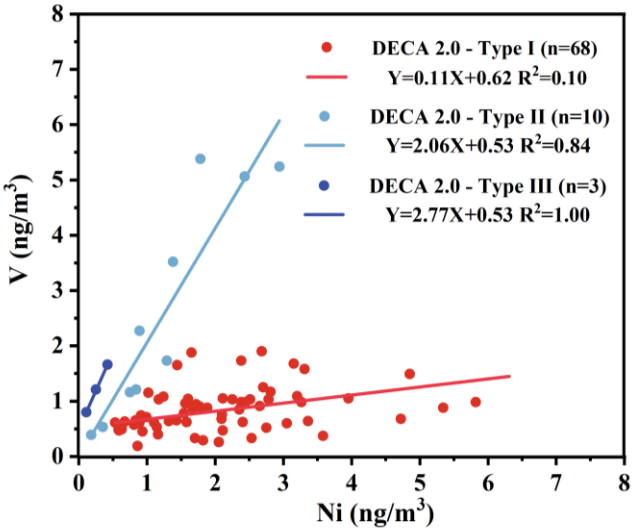

Figure 5. K-means clustering and their linear regression between V and Ni at observation site during DECA 2.0.

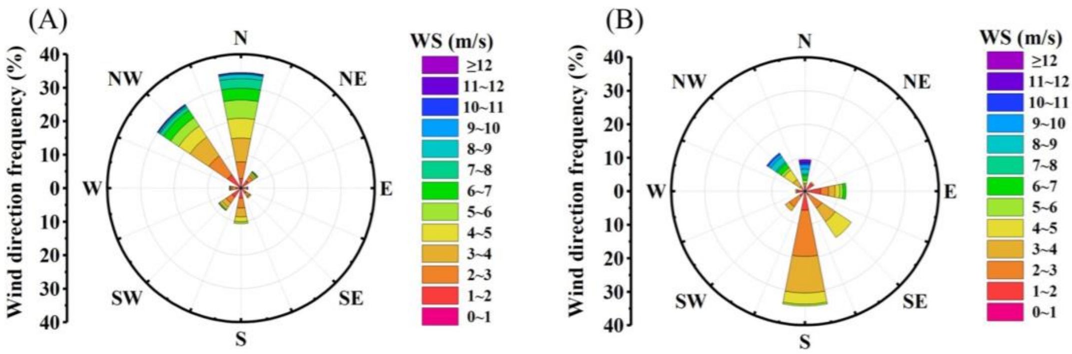

Figure 6. *Cont.*

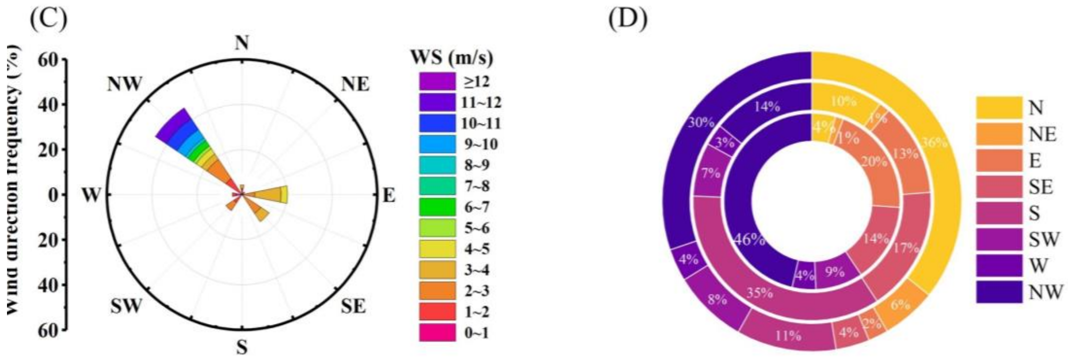

Figure 6. Wind rose under Types I (**A**), Types II (**B**), Types III (**C**), and annular wind frequency (**D**) in the DECA 2.0 stage. Outer circle: Type I. Middle circle: Type II. Inner circle: Type III.

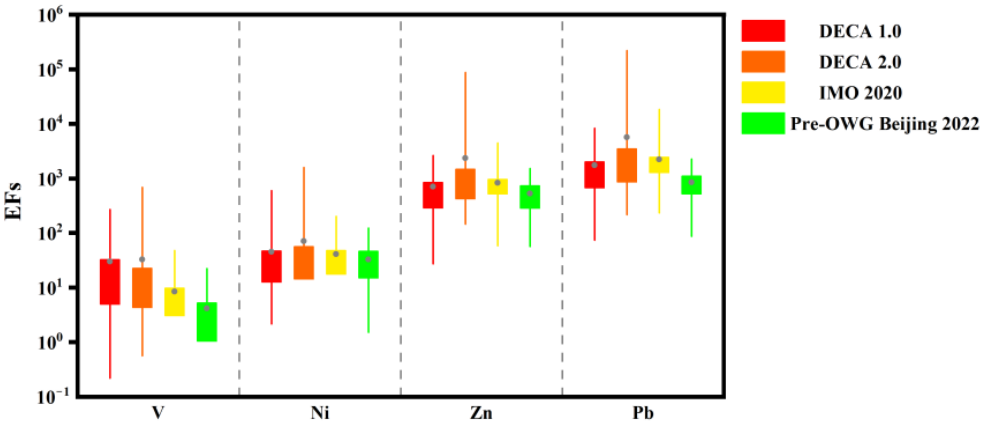

Figure 7. EF values of trace elements in PM_1 under different policies.

3.3. Airflow Backward Trajectory

The airflow backward trajectory analysis was carried out for different shipping policy stages, and three trajectories were clustered (Figure 8). Cluster 1 originated in the central part of Shandong Province, a typical local transport, which was also affected by the atmosphere over Bohai Bay during local transmission. Cluster 2 had a moderate-distance transport. The contribution of cluster 2 ranged from 22.8% to 29.4%, mainly originating from Mongolia, central Inner Mongolia, China. The air mass arrived in Qingdao from Hebei Province, Beijing, Tianjin, and other heavily polluted regions and passed through the Bohai Bay. Cluster 3 had long-distance transport, originating from Russia and Mongolia, with relative contribution of air mass from 28.5% to 38.0%.

The V concentrations of Cluster 1 in DECA 1.0, DECA 2.0, IMO 2020, and Pre-OWG Beijing 2022 were 4.01 ± 2.80, 1.50 ± 1.40, 1.07 ± 0.75, and 0.85 ± 0.72 ng/m^3, respectively (Table 7). Compared with Cluster 1, the V concentrations of Cluster 2 under different shipping policies decreased by 26.2%, 26.0%, 33.6%, and 37.6%, respectively. The V concentrations of Cluster 3 under different shipping policies decreased by 27.2%, 54.7%, 43.0%, and 36.1%, respectively. The V concentrations of Cluster 3 decreased significantly in the DECA 2.0 and IMO 2020 stage compared with the DECA 1.0 stage. The results showed that local ship emission sources contributed more to V.

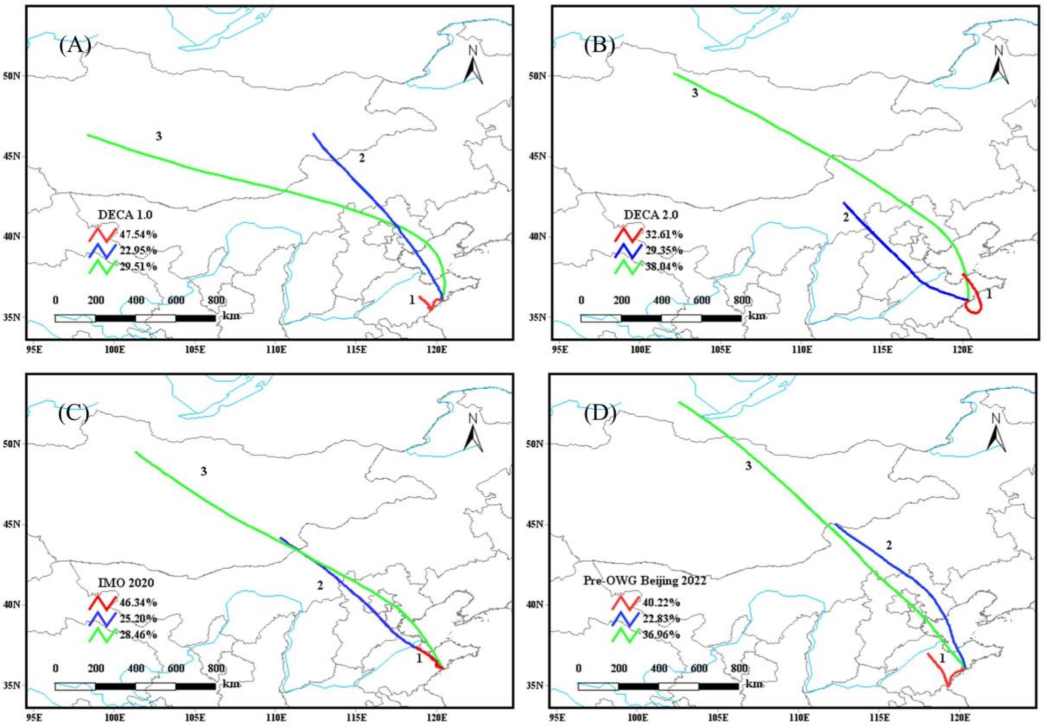

Figure 8. Trajectory of 48 h airflow in DECA 1.0 (**A**), DECA 2.0 (**B**), IMO 2020 (**C**), and Pre-OWG Beijing 2022 (**D**).

Table 7. V, Ni, Zn, and Pb and their ratios in PM_1 under different air mass trajectories and policies.

Cluster Types	Policy Stages	Samples	V (ng/m³)	Ni (ng/m³)	Zn (ng/m³)	Pb (ng/m³)	V/Ni	V/Zn	V/Pb
Cluster 1	DECA 1.0	29	4.01 ± 2.80	3.03 ± 1.78	77.5 ± 60.6	23.3 ± 14.2	1.29 ± 0.73	0.08 ± 0.10	0.21 ± 0.18
	DECA 2.0	22	1.50 ± 1.40	2.13 ± 1.26	63.7 ± 56.2	18.4 ± 15.6	1.17 ± 1.38	0.10 ± 0.16	0.38 ± 0.61
	IMO 2020	46	1.07 ± 0.75	3.55 ± 2.70	71.0 ± 47.2	22.8 ± 14.6	0.36 ± 0.25	0.04 ± 0.11	0.10 ± 0.17
	Pre-OWG Beijing 2022	34	0.85 ± 0.72	4.21 ± 2.42	78.7 ± 58.2	15.0 ± 6.85	0.23 ± 0.21	0.02 ± 0.10	0.08 ± 0.04
Cluster 2	DECA 1.0	17	2.96 ± 3.00	3.70 ± 3.30	58.8 ± 33.5	18.1 ± 9.95	0.86 ± 0.66	0.20 ± 0.24	0.06 ± 0.08
	DECA 2.0	22	1.11 ± 1.04	2.35 ± 1.15	68.4 ± 40.7	20.0 ± 11.9	0.66 ± 0.58	0.02 ± 0.03	0.09 ± 0.11
	IMO 2020	26	0.71 ± 0.43	2.53 ± 1.42	68.2 ± 29.6	22.4 ± 8.82	0.31 ± 0.16	0.01 ± 0.01	0.03 ± 0.02
	Pre-OWG Beijing 2022	14	0.53 ± 0.54	3.73 ± 3.18	64.5 ± 27.4	12.9 ± 5.12	0.17 ± 0.17	0.01 ± 0.06	0.05 ± 0.01
Cluster 3	DECA 1.0	15	2.92 ± 3.35	1.89 ± 1.62	48.2 ± 41.4	15.6 ± 13.8	1.15 ± 0.96	0.18 ± 0.19	0.06 ± 0.08
	DECA 2.0	26	0.68 ± 0.31	1.37 ± 1.00	48.6 ± 51.2	10.6 ± 6.65	0.91 ± 1.45	0.02 ± 0.03	0.10 ± 0.11
	IMO 2020	29	0.61 ± 0.41	2.23 ± 2.41	51.7 ± 26.3	16.9 ± 7.45	0.37 ± 0.27	0.02 ± 0.03	0.05 ± 0.07
	Pre-OWG Beijing 2022	33	0.55 ± 0.47	2.83 ± 1.90	51.8 ± 36.2	10.3 ± 6.04	0.22 ± 0.15	0.01 ± 0.05	0.06 ± 0.01

The long-distance air mass transport in the DECA 2.0 and IMO 2020 stages contributes less to V concentrations in ports such as Tianjin Port and Tangshan Port [20]. The characteristics of V concentration under different airflows (oceanic airflow, inland airflow, and mixed airflow) in Jingtang Port were investigated. The results showed that oceanic airflow significantly impacted coastal areas. The vessel switched fuels, and low-sulfur fuel reduced the vessel-related V by 97.1% [20,60]. The transmission distance was positively correlated with PM_1 concentration. The closer the air mass transport distance, the greater the PM_1 concentration [31]. The Ni, Pb, and Zn concentrations had similar characteristics during the observation period. The changes in the concentration of V in the DECA 1.0 and DECA 2.0 stages did not have the change rules, but the same changes occurred in the IMO 2020 and Pre-OWG Beijing 2022 stages. The transmission of inland air masses, which brought V from industrial sources, might affect the sampling site. The findings by Bi et al. (2019) [86] also showed that V was primarily derived from coal combustion and motor vehicle emissions.

The V/Ni ratios of Cluster 1 to Cluster 3 in the DECA 1.0 stage were 1.29 ± 0.73, 0.86 ± 0.66, and 1.15 ± 0.96, respectively. The V/Ni ratios of Cluster 1 to Cluster 3 in the DECA 2.0 stage were 1.17 ± 1.38, 0.66 ± 0.58, and 0.91 ± 1.45, respectively. Compared with the DECA 2.0 stage, the V/Ni ratio of Cluster 1 to Cluster 3 in IMO 2020 decreased by 69.2%, 53.0%, and 59.3%, respectively. Compared with the DECA 1.0 stage, the V/Ni ratio in Cluster 3 slightly dropped in the DECA 2.0 stage and dramatically dropped in the IMO 2020 stage. In the DECA 2.0 stage, the V/Pb ratio of different air mass trajectories (Cluster 1 to Cluster 3) were 0.38 ± 0.61, 0.09 ± 0.11, and 0.10 ± 0.11, respectively, which were higher than the V/Pb ratio of other shipping policy stages. The V/Ni ratio of Cluster 1 (1.17 ± 1.38) was higher than that of Cluster 3 (0.91 ± 1.45) in the DECA 2.0 stage (Table 7), indicating that the global low-sulfur fuel oil replacement target had not been fully implemented, especially for the ships 12 nautical miles away from the coastline. There were still a number of ships using high-sulfur fuel oil. In addition, there might be regulatory loopholes in the implementation stage of DECA 2.0, and a number of ships used heavy fuel oil and low-sulfur fuel oil alternately offshore. Ships' evasion tactics have become another obstacle to achieving the desired emissions reductions [87]. Alongside this, the contribution of inland transportation to V and Ni gradually increased, but the influence of ship sources weakened [31].

The PSCF results showed that V might distributed in Qingdao and the surrounding coastal areas in the DECA 1.0 stage. Coastal cities such as Tianjin, Yantai, and Rizhao had higher V and similar potential emission source areas to Ni (Figure 9A,E). The potential emission source area of V reduced in the DECA 2.0 stage, mainly distributed in Qingdao and its coastal regions (Figure 9B). The potential emission areas of V and Ni in the IMO 2020 stage were widely distributed in inland areas (Figure 9C,G). The potential emission area of the Pre-OWG Beijing 2022 stage was significantly reduced, mainly concentrated in Qingdao (Figure 9D,H), though V and Ni were still high in several inland cities. A series of stringent control measures were implemented in BTH and surrounding areas to ensure air quality improvement before and during the Beijing Winter Olympics, which might have significantly reduced the potential emission areas of SO_2, V, and Ni (Figure S9).

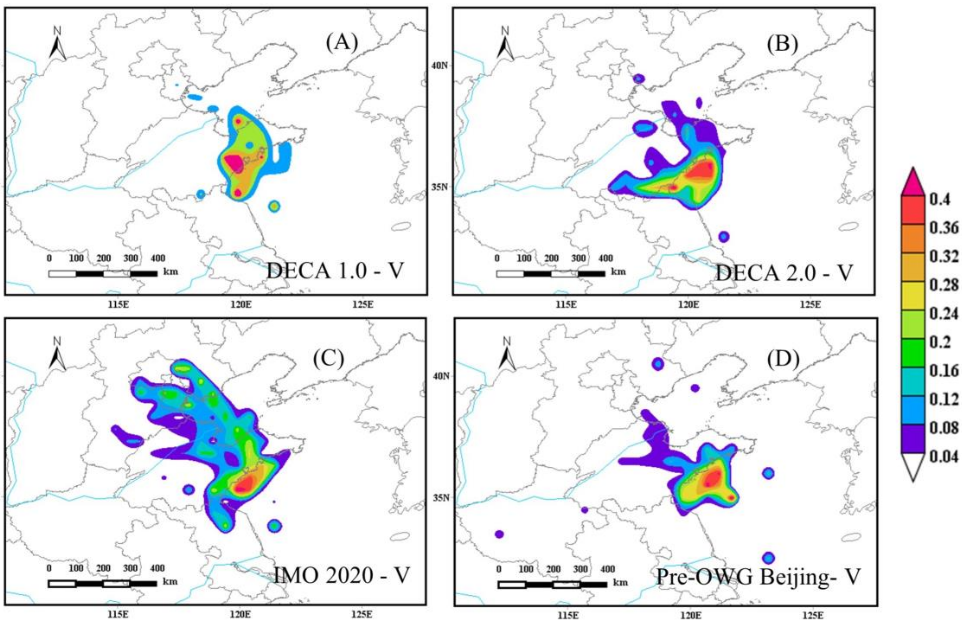

Figure 9. *Cont.*

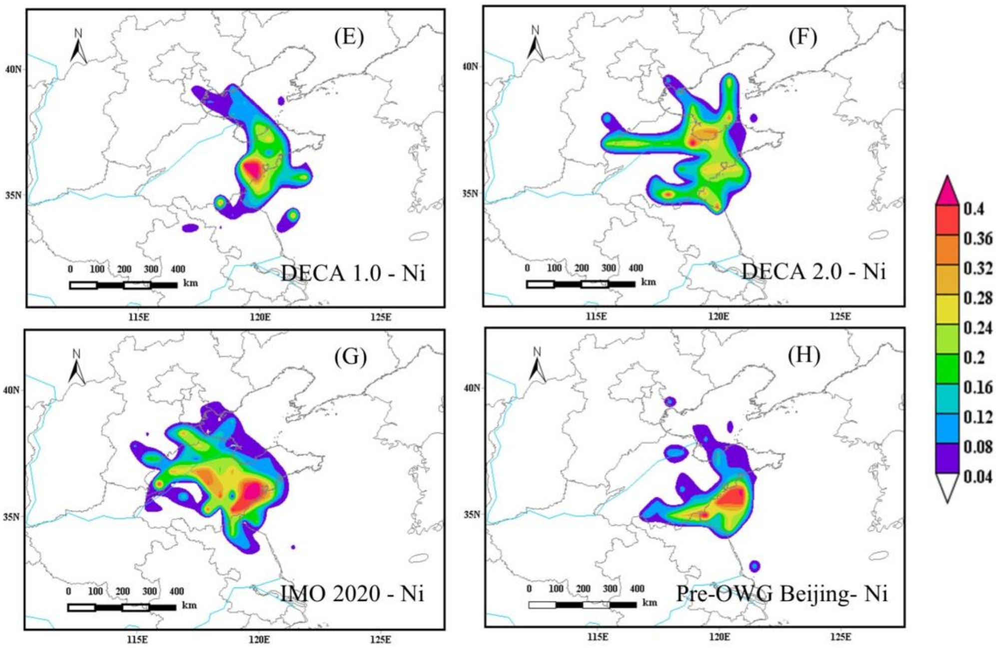

Figure 9. Potential source areas of V and Ni in PM_1. Sources areas of V in DECA 1.0 (**A**), DECA 2.0 (**B**), IMO 2020 (**C**), and Pre-OWG Beijing 2022 (**D**). Sources areas of Ni in DECA 1.0 (**E**), DECA 2.0 (**F**), IMO 2020 (**G**), and Pre-OWG Beijing 2022 (**H**).

3.4. Impact of Ship Emissions on Coastal SO_2

An important effect of the emission reductions in SOx and NOx is the resulting reduction in atmospheric concentrations of PM, especially secondary particulate sulfate and nitrate [88]. High-sulfur heavy sulfur oil burned by ships emits 9.5 million tons > of sulfur oxides into the atmosphere each year [89]. Sofiev et al. (2018) have shown that the global limit on sulfur content in ship fuels decreases concentrations of particulate sulfate by 2–4 $\mu g/m^3$ in the vicinity of busy ship lanes on a worldwide scale, leading to significant reductions in $PM_{2.5}$ [90]. Different trace elements in PM_1 can be used as tracers of pollution sources [91]. Previous studies have shown that As was a tracer element for coal combustion sources, Cr was a tracer element for industrial sources, and V was a tracer element for ship sources [9,37,53,70,91,92]. The relative contribution of each pollution source to SO_2 during the observation period was explored, and the multi-linear regression model was as follows:

$$[SO_2] = \beta_1 \times [As] + \beta_2 \times [Cr] + \beta_3 \times [V] + \beta_4 \quad (6)$$

$$[SO_2] = 761.0[As] + 865[Cr] + 162[V] + 5732 \quad (7)$$

$$[SO_2] = 2529[As] - 1.40 \times 10^{-13}[Cr] - 1.46 \times 10^{-6}[V] + 7255 \quad (8)$$

$$[SO_2] = 1496[As] + 1181[Cr] + 7.82 \times 10^{-14}[V] + 5839 \quad (9)$$

$$[SO_2] = 1101[As] - 8.09 \times 10^{-11}[Cr] - 7.27 \times 10^{-4}[V] + 5996 \quad (10)$$

In the equation, SO_2 comes from four sources: coal combustion ([As]), industrial emission ([Cr]), ship emission ([V]), and background concentration (β_4). β_1, β_2, and β_3 were correlation coefficients of linear regression. The equations for the multiple linear regression curves for the different policies are shown, where DECA 1.0 is Equation (7), DECA 2.0 is Equation (8), IMO2020 is Equation (9), and Pre-OWG Beijing 2022 is Equation (10).

The multivariate linear curve in the DECA 1.0 stage showed a better fitting result (Figure 10). The coal-fired source had the most significant influence on SO_2 concentration during the observation period. The contribution of ship sources in the DECA 1.0 stage is 1.8%, much higher than other stages. After the implementation of DECA 2.0, the indication effect of V as a shipping source was reduced. Previous observations conducted in Qingdao showed that coal-burning sources contribute more to urban pollution than mobile and industrial sources in winter [31,37]. SO_2 dropped significantly in the Pre-OWG Beijing 2022 stage, which is related to the strict coal combustion restriction policy for BTH areas before the Beijing Winter Olympics.

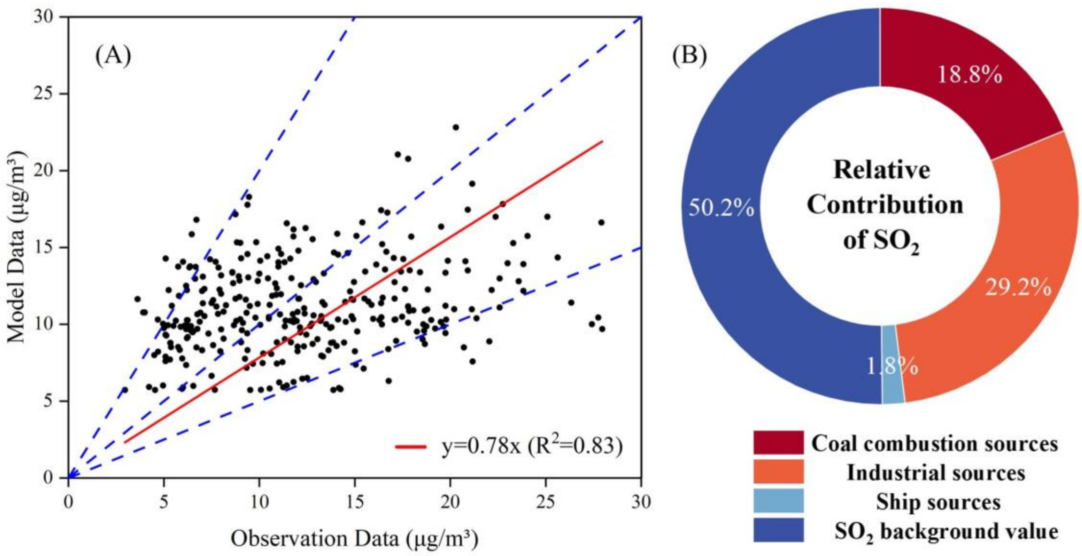

Figure 10. Linear regression of SO_2 simulated values on observed values (**A**) and relative contribution of each source to SO_2 (**B**) during the DECA 1.0 stage.

4. Conclusions

A four-year autumn and winter observation was carried out in Qingdao, a coastal megacity of northern China, from 2018 to 2022. V, Ni, Pb, and Zn characteristics and their ratios in PM_1 under different shipping policies were investigated. The ship emission source dominated the V/Ni ratio in the DECA 1.0 stage, and the V/Ni ratio was gradually affected by the inland source after implementing DECA 2.0. The indication effect of V as a shipping source was reduced and has been affected by other emission sources since 2019.

The V/Ni ratio of Type I in the DECA 2.0 stage was lower than that of Type II, which was related to the influence of meteorological factors. The high V/Ni ratios were mainly due to transmission from the southeastern marine sources to Qingdao. The high V/Ni ratios due to low Ni concentrations from inland transport can be misleading when using V/Ni ratios to identify ship emission sources.

The V/Ni ratio of the local air mass transmission was higher than that of the long-distance transmission. This indicated that some ships still used high-sulfur fuel oil, especially vessels 12 nautical miles from the coastline during the DECA 2.0 stage. The global low-sulfur fuel oil replacement target had yet to be fully implemented in the DECA 2.0 stage.

Alongside this, the contribution of inland transportation to V and Ni gradually increased. Based on the multiple linear regression model, the DECA 1.0 phase showed a better fit using V as a tracer for ship emission sources to ambient SO_2. After the DECA 2.0 stage, the fitting coefficients for V as a shipping source could be ignored due to the influence of other emission sources.

Supplementary Materials: The following supporting information can be downloaded at: https://www.mdpi.com/article/10.3390/atmos15030264/s1, Figure S1: Domestic vessel emission control areas regulated by the MOT; Figure S2: Evolution of sulfur content requirements for fuels in DECAs in China; Figure S3: The aggregated annual amount of each type of fuel oil consumed by all ships of 5000 GT and above from 2019 to 2021; Figure S4: Time series of wind speed, relative humidity, temperature, and visibility during observation; Figure S5: Time series of PM1 concentrations during observation; Figure S6: Monthly cargo throughput, foreign trade cargo throughput, and container throughput of port in Qingdao; Figure S7: Yearly development of LNG-fueled fleet; Figure S8:

Correlation coefficients of trace elements during DECA 1.0 (A), DECA 2.0 (B), IMO 2020 (C), and Pre-OWG Beijing 2022 (D); Figure S9: Potential emission areas of SO2 in PM1 in DECA 1.0 (A), DECA 2.0 (B), IMO 2020 (C), and Pre-OWG Beijing 2022 (D); Table S1: Ratio of secondary dissolution concentration of metal elements in PM1 to blank sample concentration.

Author Contributions: Conceptualization, W.G., Y.L., L.X., Y.S. and Y.Z.; methodology, J.D., Z.L., W.G., Y.L., L.X. and Y.Z.; formal analysis, J.D., Z.L. and W.T.; investigation, J.D., Z.L., J.Y., C.W. and Y.Z.; resources, T.W., J.Z., L.X., H.Z., F.W. and Y.Z.; data curation, J.D., Z.L. and W.T.; writing—original draft preparation, Z.L. and W.T.; writing—review and editing, J.D. and Y.Z.; visualization, C.W.; supervision, Y.S. and Y.Z. All authors have read and agreed to the published version of the manuscript.

Funding: This research was funded by the Municipal Nature Science Foundation in Shandong (ZR2023MD056), the Research Fund Program of Guangdong-Hongkong-Macau Joint Laboratory of Collaborative Innovation for Environmental Quality (GHML2021-103), and the Open Project Fund of First-Class Discipline of Environmental Science and Engineering in Shandong (QUTSEME201911).

Institutional Review Board Statement: Not applicable.

Informed Consent Statement: Not applicable.

Data Availability Statement: The data presented in this study are available upon request from the corresponding author. The data are not publicly available due to privacy.

Acknowledgments: The authors acknowledge the support received from Xiaohuan Liu from Ocean University of China. Five anonymous reviewers provided helpful and constructive comments that improved the manuscript substantially.

Conflicts of Interest: Author Fei Wang were employed by the SunRui Marine Environment Engineering Co., Ltd. The remaining authors declare that the research was conducted in the absence of any commercial or financial relationships that could be construed as a potential conflict of interest.

References

1. Manshausen, P.; Watson-Parris, D.; Christensen, M.W.; Jalkanen, J.P.; Stier, P. Invisible ship tracks show large cloud sensitivity to aerosol. *Nature* **2022**, *610*, 101–106. [CrossRef]
2. Jang, E.; Choi, S.; Yoo, E.; Hyun, S.; An, J. Impact of shipping emissions regulation on urban aerosol composition changes revealed by receptor and numerical modelling. *NPJ Clim. Atmos. Sci.* **2023**, *6*, 52. [CrossRef]
3. Toscano, D. The impact of shipping on air quality in the port cities of the Mediterranean Area: A review. *Atmosphere* **2023**, *14*, 1180. [CrossRef]
4. Liu, H.; Fu, M.; Jin, X.; Shang, Y.; Shindell, D.; Faluvegi, G.; Shindell, C.; He, K. Health and climate impacts of ocean-going vessels in East Asia. *Nat. Clim. Chang.* **2016**, *6*, 1037–1041. [CrossRef]
5. Tian, L.; Ho, K.-f.; Louie, P.K.K.; Qiu, H.; Pun, V.C.; Kan, H.; Yu, I.T.S.; Wong, T.W. Shipping emissions associated with increased cardiovascular hospitalizations. *Atmos. Environ.* **2013**, *74*, 320–325. [CrossRef]
6. Fan, Q.; Zhang, Y.; Ma, W.; Ma, H.; Feng, J.; Yu, Q.; Yang, X.; Ng, S.K.W.; Fu, Q.; Chen, L. Spatial and seasonal dynamics of ship emissions over the Yangtze River Delta and East China Sea and their potential environmental influence. *Environ. Sci. Technol.* **2016**, *50*, 1322–1329. [CrossRef]
7. Wang, X.; Yi, W.; Lv, Z.; Deng, F.; Zheng, S.; Xu, H.; Zhao, J.; Liu, H.; He, K. Ship emissions around China under gradually promoted control policies from 2016 to 2019. *Atmos. Chem. Phys.* **2021**, *21*, 13835–13853. [CrossRef]
8. Lv, Z.; Liu, H.; Ying, Q.; Fu, M.; Meng, Z.; Wang, Y.; Wei, W.; Gong, H.; He, K. Impacts of shipping emissions on $PM_{2.5}$ pollution in China. *Atmos. Chem. Phys.* **2018**, *18*, 15811–15824. [CrossRef]
9. Feng, X.; Ma, Y.; Lin, H.; Fu, T.; Zhang, Y.; Wang, X.; Zhang, A.; Yuan, Y.; Han, Z.; Mao, J.; et al. Impacts of ship emissions on air quality in southern China: Opportunistic insights from the abrupt emission changes in early 2020. *Environ. Sci. Technol.* **2023**, *57*, 16999–17010. [CrossRef]
10. Zhai, J.; Yu, G.; Zhang, J.; Shi, S.; Yuan, Y.; Jiang, S.; Xing, C.; Cai, B.; Zeng, Y.; Wang, Y.; et al. Impact of ship emissions on air quality in the greater bay area in China under the latest global marine fuel regulation. *Environ. Sci. Technol.* **2023**, *57*, 12341–12350. [CrossRef]
11. Yuan, C.; Wong, K.W.; Tseng, Y.; Ceng, J.; Lee, C.; Lin, C. Chemical significance and source apportionment of fine particles ($PM_{2.5}$) in an industrial port area in East Asia. *Atmos. Pollut. Res.* **2022**, *13*, 101349. [CrossRef]
12. Deng, M.; Peng, S.; Xie, X.; Jiang, Z.; Hu, J.; Qi, Z.; Sun, J. SO_2 compliance monitoring and emission characteristics analysis of navigating ships: A case study of Shanghai waters in emission control areas, China. *Atmos. Pollut. Res.* **2022**, *13*, 101560. [CrossRef]

13. Mandal, A.; Biswas, J.; Farooqui, Z.; Roychowdhury, S. A detailed perspective of marine emissions and their environmental impact in a representative Indian port. *Atmos. Pollut. Res.* **2021**, *12*, 101194. [CrossRef]
14. Van, T.C.; Ramirez, J.; Rainey, T.; Ristovski, Z.; Brown, R.J. Global impacts of recent IMO regulations on marine fuel oil refining processes and ship emissions. *Transp. Res. D Transp. Environ.* **2019**, *70*, 123–134. [CrossRef]
15. Carr, E.W.; Corbett, J.J. Ship Compliance in Emission Control Areas: Technology Costs and Policy Instruments. *Environ. Sci. Technol.* **2015**, *49*, 9584–9591. [CrossRef]
16. Spada, N.J.; Cheng, X.; White, W.H.; Hyslop, N.P. Decreasing Vanadium Footprint of Bunker Fuel Emissions. *Environ. Sci. Technol.* **2018**, *52*, 11528–11534. [CrossRef]
17. Yang, L.; Zhang, Q.; Lv, Z.; Zhang, Y.; Yang, Z.; Fu, F.; Lv, J.; Wu, L.; Mao, H. Efficiency of DECA on ship emission and urban air quality: A case study of China port. *J. Clean. Prod.* **2022**, *362*, 132556. [CrossRef]
18. Viana, M.; Amato, F.; Alastuey, A.; Querol, X.; Moreno, T.; García Dos Santos, S.; Herce, M.D.; Fernández-Patier, R. Chemical tracers of particulate emissions from commercial shipping. *Environ. Sci. Technol.* **2009**, *43*, 7472–7477. [CrossRef] [PubMed]
19. Liu, H.; Jin, X.; Wu, L.; Wang, X.; Fu, M.; Lv, Z.; Morawska, L.; Huang, F.; He, K. The impact of marine shipping and its DECA control on air quality in the Pearl River Delta, China. *Sci. Total Environ.* **2018**, *625*, 1476–1485. [CrossRef]
20. Zhang, Y.; Deng, F.; Man, H.; Fu, M.; Lv, Z.; Xiao, Q.; Jin, X.; Liu, S.; He, K.; Liu, H. Compliance and port air quality features with respect to ship fuel switching regulation: A field observation campaign, SEISO-Bohai. *Atmos. Chem. Phys.* **2019**, *19*, 4899–4916. [CrossRef]
21. Zhang, X.; Zhang, Y.; Liu, Y.; Zhao, J.; Zhou, Y.; Wang, X.; Yang, X.; Zou, Z.; Zhang, C.; Fu, Q.; et al. Changes in the SO_2 level and $PM_{2.5}$ components in Shanghai driven by Implementing the ship emission control policy. *Environ. Sci. Technol.* **2019**, *53*, 11580–11587. [CrossRef]
22. Zou, Z.; Zhao, J.; Zhang, C.; Zhang, Y.; Yang, X.; Chen, J.; Xu, J.; Xue, R.; Zhou, B. Effects of cleaner ship fuels on air quality and implications for future policy: A case study of Chongming Ecological Island in China. *J. Clean. Prod.* **2020**, *267*, 122088. [CrossRef]
23. Zhao, S.; Tian, H.; Luo, L.; Liu, H.; Wu, B.; Liu, S.; Bai, X.; Liu, W.; Liu, X.; Wu, Y.; et al. Temporal variation characteristics and source apportionment of metal elements in $PM_{2.5}$ in urban Beijing during 2018–2019. *Environ. Pollut.* **2021**, *268*, 115856. [CrossRef] [PubMed]
24. Agrawal, H.; Welch, W.A.; Miller, J.W.; Cocker, D.R. Emission measurements from a crude oil tanker at sea. *Environ. Sci. Technol.* **2008**, *42*, 7098–7103. [CrossRef] [PubMed]
25. Agrawal, H.; Eden, R.; Zhang, X.; Fine, P.M.; Katzenstein, A.; Miller, J.W.; Ospital, J.; Teffera, S.; Cocker, D.R. Primary particulate matter from ocean-going engines in the Southern California air basin. *Environ. Sci. Technol.* **2009**, *43*, 5398–5402. [CrossRef]
26. Celo, V.; Dabek-Zlotorzynska, E.; McCurdy, M. Chemical characterization of exhaust emissions from selected Canadian marine vessels: The case of trace metals and lanthanoids. *Environ. Sci. Technol.* **2015**, *49*, 5220–5226. [CrossRef]
27. Corbin, J.C.; Mensah, A.A.; Pieber, S.M.; Orasche, J.; Michalke, B.; Zanatta, M.; Czech, H.; Massabò, D.; Buatier de Mongeot, F.; Mennucci, C.; et al. Trace metals in soot and $PM_{2.5}$ from heavy-fuel-oil combustion in a marine engine. *Environ. Sci. Technol.* **2018**, *52*, 6714–6722. [CrossRef]
28. John, S.G.; Kelly, R.L.; Bian, X.; Fu, F.; Smith, I.; Lanning, N.T.; Liang, H.; Pasquier, B.; Seelen, E.; Holzer, M.; et al. The biogeochemical balance of oceanic nickel cycling. *Nat. Geosci.* **2022**, *15*, 906–912. [CrossRef]
29. Zhang, B.; Zhang, H.; He, J.; Zhou, S.; Dong, H.; Rinklebe, J.; Ok, Y.S. Vanadium in the Environment: Biogeochemistry and Bioremediation. *Environ. Sci. Technol.* **2023**, *57*, 14770–14786. [CrossRef] [PubMed]
30. Yu, G.; Zhang, Y.; Yang, F.; He, B.; Zhang, C.; Zou, Z.; Yang, X.; Li, N.; Chen, J. Dynamic Ni/V ratio in the ship-emitted particles driven by multiphase fuel oil regulations in coastal China. *Environ. Sci. Technol.* **2021**, *55*, 15031–15039. [CrossRef]
31. Liu, Z.; Zhang, H.; Zhang, Y.; Liu, X.; Ma, Z.; Xue, L.; Peng, X.; Zhao, J.; Gong, W.; Peng, Q.; et al. Characterization and sources of trace elements in PM_1 during autumn and winter in Qingdao, Northern China. *Sci. Total Environ.* **2022**, *811*, 151319. [CrossRef] [PubMed]
32. Zhao, M.; Zhang, Y.; Ma, W.; Fu, Q.; Yang, X.; Li, C.; Zhou, B.; Yu, Q.; Chen, L. Characteristics and ship traffic source identification of air pollutants in China's largest port. *Atmos. Environ.* **2013**, *64*, 277–286. [CrossRef]
33. Wang, Z.; Xu, H.; Gu, Y.; Feng, R.; Zhang, N.; Wang, Q.; Cao, J.; Liu, S.; Zhang, Q.; Liu, P.; et al. Chemical characterization of $PM_{2.5}$ in heavy polluted industrial zones in the Guanzhong Plain, northwest China: Determination of fingerprint source profiles. *Sci. Total Environ.* **2022**, *840*, 156729. [CrossRef] [PubMed]
34. Ming, L.; Jin, L.; Li, J.; Fu, P.; Yang, W.; Liu, D.; Zhang, G.; Wang, Z.; Li, X. $PM_{2.5}$ in the Yangtze River Delta, China: Chemical compositions, seasonal variations, and regional pollution events. *Environ. Pollut.* **2017**, *223*, 200–212. [CrossRef]
35. Qin, S.; Li, B.; Wang, X.; Huang, H.; Zeng, M.; Xiao, F.; Xu, X. Metal element detection and carcinogenicity risk assessment of $PM_{2.5}$ Samples. *Environ. Toxicol. Chem.* **2020**, *39*, 1273–1276. [CrossRef]
36. Liu, H.; Song, D.; Zhang, X.; Huang, F.; Hu, X. A study on characteristics of heavy metal elements in atmospheric $PM_{2.5}$ during winter in Chengdu. *IOP Conf. Ser. Earth Environ. Sci.* **2020**, *514*, 032046. [CrossRef]
37. Bie, S.; Yang, L.; Zhang, Y.; Huang, Q.; Li, J.; Zhao, T.; Zhang, X.; Wang, P.; Wang, W. Source appointment of $PM_{2.5}$ in Qingdao Port, East of China. *Sci. Total Environ.* **2021**, *755*, 142456. [CrossRef]
38. Chen, D.; Wang, X.; Nelson, P.; Li, Y.; Zhao, N.; Zhao, Y.; Lang, J.; Zhou, Y.; Guo, X. Ship emission inventory and its impact on the $PM_{2.5}$ air pollution in Qingdao Port, North China. *Atmos. Environ.* **2017**, *166*, 351–361. [CrossRef]

39. MOT, Ministry of Transport of China. Available online: https://www.mot.gov.cn/tongjishuju/gangkouhuowulvkettl (accessed on 20 November 2023).
40. Luo, H.; Wang, Q.; Guan, Q.; Ma, Y.; Ni, F.; Yang, E.; Zhang, J. Heavy metal pollution levels, source apportionment and risk assessment in dust storms in key cities in Northwest China. *J. Hazard. Mater.* **2022**, *422*, 126878. [CrossRef] [PubMed]
41. Xu, H.; Wang, Y.; Liu, R.; Wang, M.; Zhang, Y. Spatial distribution, chemical speciation and health risk of heavy metals from settled dust in Qingdao urban area. *Atmosphere* **2019**, *10*, 73. [CrossRef]
42. Cesari, D.; De Benedetto, G.E.; Bonasoni, P.; Busetto, M.; Dinoi, A.; Merico, E.; Chirizzi, D.; Cristofanelli, P.; Donateo, A.; Grasso, F.M.; et al. Seasonal variability of $PM_{2.5}$ and PM_{10} composition and sources in an urban background site in Southern Italy. *Sci. Total Environ.* **2018**, *612*, 202–213. [CrossRef]
43. Islam, N.; Dihingia, A.; Khare, P.; Saikia, B.K. Atmospheric particulate matters in an Indian urban area: Health implications from potentially hazardous elements, cytotoxicity, and genotoxicity studies. *J. Hazard. Mater.* **2020**, *384*, 121472. [CrossRef] [PubMed]
44. Wu, R.; Zhou, X.; Wang, L.; Wang, Z.; Zhou, Y.; Zhang, J.; Wang, W. $PM_{2.5}$ characteristics in Qingdao and across coastal cities in China. *Atmosphere* **2017**, *8*, 77. [CrossRef]
45. Zhang, Y.; Lang, J.; Cheng, S.; Li, S.; Zhou, Y.; Chen, D.; Zhang, H.; Wang, H. Chemical composition and sources of PM_1 and $PM_{2.5}$ in Beijing in autumn. *Sci. Total Environ.* **2018**, *630*, 72–82. [CrossRef]
46. Zeng, P.; Huang, X.; Yan, M.; Zheng, Z.; Qiu, Z.; Yun, L.; Lin, C.; Zhang, L. Ambient Ozone and Fine Particular Matter Pollution in a Megacity in South China: Trends, Concurrent Pollution, and Health Risk Assessment. *Atmosphere* **2023**, *14*, 1806. [CrossRef]
47. Khan, J.Z.; Sun, L.; Tian, Y.; Shi, G.; Feng, Y. Chemical characterization and source apportionment of PM_1 and $PM_{2.5}$ in Tianjin, China: Impacts of biomass burning and primary biogenic sources. *J. Environ. Sci.* **2021**, *99*, 196–209. [CrossRef] [PubMed]
48. Squizzato, S.; Masiol, M.; Agostini, C.; Visin, F.; Formenton, G.; Harrison, R.M.; Rampazzo, G. Factors, origin and sources affecting PM_1 concentrations and composition at an urban background site. *Atmos. Res.* **2016**, *180*, 262–273. [CrossRef]
49. Sarti, E.; Pasti, L.; Rossi, M.; Ascanelli, M.; Pagnoni, A.; Trombini, M.; Remelli, M. The composition of PM_1 and $PM_{2.5}$ samples, metals and their water soluble fractions in the Bologna area (Italy). *Atmos. Pollut. Res.* **2015**, *6*, 708–718. [CrossRef]
50. Perrone, M.R.; Becagli, S.; Garcia Orza, J.A.; Vecchi, R.; Dinoi, A.; Udisti, R.; Cabello, M. The impact of long-range-transport on PM_1 and $PM_{2.5}$ at a Central Mediterranean site. *Atmos. Environ.* **2013**, *71*, 176–186. [CrossRef]
51. Shen, Z.; Cao, J.; Arimoto, R.; Han, Y.; Zhu, C.; Tian, J.; Liu, S. Chemical characteristics of fine particles (PM_1) from Xi'an, China. *Aerosol Sci. Technol.* **2010**, *44*, 461–472. [CrossRef]
52. Cheng, H.; Gong, W.; Wang, Z.; Zhang, F.; Wang, X.; Lv, X.; Liu, J.; Fu, X.; Zhang, G. Ionic composition of submicron particles ($PM_{1.0}$) during the long-lasting haze period in January 2013 in Wuhan, central China. *J. Environ. Sci.* **2014**, *26*, 810–817. [CrossRef] [PubMed]
53. Jeong, J.H.; Shon, Z.H.; Kang, M.; Song, S.K.; Kim, Y.K.; Park, J.; Kim, H. Comparison of source apportionment of $PM_{2.5}$ using receptor models in the main hub port city of East Asia: Busan. *Atmos. Environ.* **2017**, *148*, 115–127. [CrossRef]
54. Mamoudou, I.; Zhang, F.; Chen, Q.; Wang, P.; Chen, Y. Characteristics of $PM_{2.5}$ from ship emissions and their impacts on the ambient air: A case study in Yangshan Harbor, Shanghai. *Sci. Total Environ.* **2018**, *640–641*, 207–216. [CrossRef] [PubMed]
55. Tao, J.; Zhang, L.; Cao, J.; Zhong, L.; Chen, D.; Yang, Y.; Chen, D.; Chen, L.; Zhang, Z.; Wu, Y.; et al. Source apportionment of $PM_{2.5}$ at urban and suburban areas of the Pearl River Delta region, south China—With emphasis on ship emissions. *Sci. Total Environ.* **2017**, *574*, 1559–1570. [CrossRef] [PubMed]
56. Zhang, F.; Chen, Y.; Tian, C.; Wang, X.; Huang, G.; Fang, Y.; Zong, Z. Identification and quantification of shipping emissions in Bohai Rim, China. *Sci. Total Environ.* **2014**, *497–498*, 570–577. [CrossRef]
57. Cheng, K.; Chang, Y.; Kuang, Y.; Ling, Q.; Zou, Z.; Huang, R.-J. Multiple-Year Changes (2014–2018) in Particulate Vanadium Linked to Shipping Regulations in the World's Largest Port Region. *ACS Earth Space Chem.* **2022**, *6*, 415–420. [CrossRef]
58. MEPC. *2019 Report of Fuel Oil Consumption Data Submitted to the IMO Ship Fuel Oil Consumption Database in GISIS*; MEPC: London, UK, 2020; pp. 7–8. Available online: https://www.imo.org/ (accessed on 20 November 2023).
59. MEPC. *2020 Report of Fuel Oil Consumption Data Submitted to the IMO Ship Fuel Oil Consumption Database in GISIS*; MEPC: London, UK, 2021; pp. 7–8. Available online: https://www.imo.org/ (accessed on 20 November 2023).
60. Zhou, L.; Li, M.; Cheng, C.; Zhou, Z.; Nian, H.; Tang, R.; Chan, C.K. Real-time chemical characterization of single ambient particles at a port city in Chinese domestic emission control area—Impacts of ship emissions on urban air quality. *Sci. Total Environ.* **2022**, *819*, 153117. [CrossRef]
61. Ray, I.; Das, R.; Chua, S.L.; Wang, X. Seasonal variation of atmospheric Pb sources in Singapore—Elemental and lead isotopic compositions of PM_{10} as source tracer. *Chemosphere* **2022**, *307*, 136029. [CrossRef]
62. Liu, L.; Liu, Y.; Wen, W.; Liang, L.; Ma, X.; Jiao, J.; Guo, K. Source Identification of trace elements in $PM_{2.5}$ at a rural site in the North China Plain. *Atmosphere* **2020**, *11*, 179. [CrossRef]
63. Liu, J.; Chen, Y.; Chao, S.; Cao, H.; Zhang, A.; Yang, Y. Emission control priority of $PM_{2.5}$-bound heavy metals in different seasons: A comprehensive analysis from health risk perspective. *Sci. Total Environ.* **2018**, *644*, 20–30. [CrossRef] [PubMed]
64. Si, R.; Xin, J.; Zhang, W.; Wen, T.; Li, S.; Ma, Y.; Wu, X.; Cao, Y.; Xu, X.; Tang, H.; et al. Environmental and health benefits of establishing a coal banning area in the Beijing-Tianjin-Hebei region of China. *Atmos. Environ.* **2021**, *247*, 118191. [CrossRef]
65. Cheng, Y.; Zou, S.; Lee, S.C.; Chow, J.; Ho, K.; Watson, J.; Han, Y.; Zhang, R.; Zhang, F.; Yau, P.; et al. Characteristics and source apportionment of PM_1 emissions at a roadside station. *J. Hazard. Mater.* **2011**, *195*, 82–91. [CrossRef] [PubMed]

66. Zhang, J.; Wei, E.; Wu, L.; Fang, X.; Li, F.; Yang, Z.; Wang, T.; Mao, H. Elemental composition and health risk assessment of PM_{10} and $PM_{2.5}$ in the roadside microenvironment in Tianjin, China. *Air. Qual. Res.* **2018**, *18*, 1817–1827. [CrossRef]
67. Si, R.; Xin, J.; Zhang, W.; Li, S.; Wen, T.; Wang, Y.; Ma, Y.; Liu, Z.; Xu, X.; Li, M.; et al. Source apportionment and health risk assessment of trace elements in the heavy industry areas of Tangshan, China. *Air Qual. Atmos. Health.* **2019**, *12*, 1303–1315. [CrossRef]
68. Win, M.S.; Zeng, J.; Yao, C.; Zhao, M.; Xiu, G.; Xie, T.; Rao, L.; Zhang, L.; Lu, H.; Liu, X.; et al. Sources of HULIS-C and its relationships with trace metals, ionic species in $PM_{2.5}$ in suburban Shanghai during haze and non-haze days. *J. Atmos. Chem.* **2020**, *77*, 63–81. [CrossRef]
69. Luo, Y.; Zhou, X.; Zhang, J.; Xiao, Y.; Wang, Z.; Zhou, Y.; Wang, W. $PM_{2.5}$ pollution in a petrochemical industry city of northern China: Seasonal variation and source apportionment. *Atmos. Res.* **2018**, *212*, 285–295. [CrossRef]
70. Tao, J.; Gao, J.; Zhang, L.; Zhang, R.; Che, H.; Zhang, Z.; Lin, Z.; Jing, J.; Cao, J.; Hsu, S.C. $PM_{2.5}$ pollution in a megacity of southwest China: Source apportionment and implication. *Atmos. Chem. Phys.* **2014**, *14*, 8679–8699. [CrossRef]
71. Gao, J.; Wang, K.; Wang, Y.; Liu, S.; Zhu, C.; Hao, J.; Liu, H.; Hua, S.; Tian, H. Temporal-spatial characteristics and source apportionment of $PM_{2.5}$ as well as its associated chemical species in the Beijing-Tianjin-Hebei region of China. *Environ. Pollut.* **2018**, *233*, 714–724. [CrossRef]
72. Yu, Y.; He, S.; Wu, X.; Zhang, C.; Yao, Y.; Liao, H.; Wang, Q.G.; Xie, M. $PM_{2.5}$ elements at an urban site in Yangtze River Delta, China: High time-resolved measurement and the application in source apportionment. *Environ. Pollut.* **2019**, *253*, 1089–1099. [CrossRef]
73. Wang, Q.; Fang, J.; Shi, W.; Dong, X. Distribution characteristics and policy-related improvements of $PM_{2.5}$ and its components in six Chinese cities. *Environ. Pollut.* **2020**, *266*, 115299. [CrossRef]
74. Qu, Y.; Liu, X.Q.; Liu, H.K.; Wang, Q.Y.; Zhu, C.S.; Zhou, Y.; Zhang, R.J.; Cao, J.J. $PM_{2.5}$ Elements in the rural area of Jing-Jin-Ji Region in China: Source identification and health risk assessment. *Aerosol Sci. Eng.* **2021**, *5*, 429–439. [CrossRef]
75. Li, X.; Yan, C.; Wang, C.; Ma, J.; Li, W.; Liu, J.; Liu, Y. $PM_{2.5}$-bound elements in Hebei Province, China: Pollution levels, source apportionment and health risks. *Sci. Total Environ.* **2022**, *806*, 150440. [CrossRef]
76. Diao, L.; Zhang, H.; Liu, B.; Dai, C.; Zhang, Y.; Dai, Q.; Bi, X.; Zhang, L.; Song, C.; Feng, Y. Health risks of inhaled selected toxic elements during the haze episodes in Shijiazhuang, China: Insight into critical risk sources. *Environ. Pollut.* **2021**, *276*, 116664. [CrossRef] [PubMed]
77. Valotto, G.; Squizzato, S.; Masiol, M.; Zannoni, D.; Visin, F.; Rampazzo, G. Elemental characterization, sources and wind dependence of PM_1 near Venice, Italy. *Atmos. Res.* **2014**, *143*, 371–379. [CrossRef]
78. Salameh, D.; Detournay, A.; Pey, J.; Pérez, N.; Liguori, F.; Saraga, D.; Bove, M.C.; Brotto, P.; Cassola, F.; Massabò, D.; et al. $PM_{2.5}$ chemical composition in five European Mediterranean cities: A 1-year study. *Atmos. Res.* **2015**, *155*, 102–117. [CrossRef]
79. Miranda, R.M.; de Fatima Andrade, M.; Dutra Ribeiro, F.N.; Mendonça Francisco, K.J.; Pérez-Martínez, P.J. Source apportionment of fine particulate matter by positive matrix factorization in the metropolitan area of São Paulo, Brazil. *J. Clean. Prod.* **2018**, *202*, 253–263. [CrossRef]
80. Nakatsubo, R.; Oshita, Y.; Aikawa, M.; Takimoto, M.; Kubo, T.; Matsumura, C.; Takaishi, Y.; Hiraki, T. Influence of marine vessel emissions on the atmospheric $PM_{2.5}$ in Japan's around the congested sea areas. *Sci. Total Environ.* **2020**, *702*, 134744. [CrossRef] [PubMed]
81. Alves, C.; Evtyugina, M.; Vicente, E.; Vicente, A.; Rienda, I.C.; de la Campa, A.S.; Tomé, M.; Duarte, I. $PM_{2.5}$ chemical composition and health risks by inhalation near a chemical complex. *J. Environ. Sci.* **2023**, *124*, 860–874. [CrossRef]
82. Wiseman, C.L.S.; Zereini, F. Characterizing metal(loid) solubility in airborne PM_{10}, $PM_{2.5}$ and PM_1 in Frankfurt, Germany using simulated lung fluids. *Atmos. Environ.* **2014**, *89*, 282–289. [CrossRef]
83. Hassanvand, M.S.; Naddafi, K.; Faridi, S.; Nabizadeh, R.; Sowlat, M.H.; Momeniha, F.; Gholampour, A.; Arhami, M.; Kashani, H.; Zare, A.; et al. Characterization of PAHs and metals in indoor/outdoor PM_{10}/$PM_{2.5}$/PM_1 in a retirement home and a school dormitory. *Sci. Total Environ.* **2015**, *527–528*, 100–110. [CrossRef]
84. Visser, S.; Slowik, J.G.; Furger, M.; Zotter, P.; Bukowiecki, N.; Canonaco, F.; Flechsig, U.; Appel, K.; Green, D.C.; Tremper, A.H.; et al. Advanced source apportionment of size-resolved trace elements at multiple sites in London during winter. *Atmos. Chem. Phys.* **2015**, *15*, 11291–11309. [CrossRef]
85. Shaltout, A.A.; Boman, J.; Alsulimane, M.E. Identification of elemental composition of $PM_{2.5}$ collected in Makkah, Saudi Arabia, using EDXRF. *X-ray Spectrom.* **2017**, *46*, 151–163. [CrossRef]
86. Bi, X.; Dai, Q.; Wu, J.; Zhang, Q.; Zhang, W.; Luo, R.; Cheng, Y.; Zhang, J.; Wang, L.; Yu, Z.; et al. Characteristics of the main primary source profiles of particulate matter across China from 1987 to 2017. *Atmos. Chem. Phys.* **2019**, *19*, 3223–3243. [CrossRef]
87. Li, L.; Pan, Y.; Gao, S.; Yang, W. An innovative model to design extreme emission control areas (ECAs) by considering ship's evasion strategy. *Ocean Coast. Manag.* **2022**, *227*, 106289. [CrossRef]
88. Ramacher, M.O.; Tang, L.; Moldanová, J.; Matthias, V.; Karl, M.; Fridell, E.; Johansson, L. The impact of ship emissions on air quality and human health in the Gothenburg area–Part II: Scenarios for 2040. *Atmos. Chem. Phys.* **2020**, *20*, 10667–10686. [CrossRef]
89. Ni, N.; Yuan, H.; Zhang, Z.; Bai, Y.; Bai, Y.; Zhu, M. Theoretical research on ship desulfurization wastewater freezing desalination system driven by waste heat. *Desalination* **2023**, *549*, 116363. [CrossRef]

90. Sofiev, M.; Winebrake, J.J.; Johansson, L.; Carr, E.W.; Prank, M.; Soares, J.; Corbett, J.J. Cleaner fuels for ships provide public health benefits with climate tradeoffs. *Nat. Commun.* **2018**, *9*, 406. [CrossRef]
91. Li, M.; Shao, M.; Li, L.-Y.; Lu, S.-H.; Chen, W.-T.; Wang, C. Quantifying the ambient formaldehyde sources utilizing tracers. *Chin. Chem. Lett.* **2014**, *25*, 1489–1491. [CrossRef]
92. Park, E.H.; Heo, J.; Kim, H.; Yi, S.M. Long term trends of chemical constituents and source contributions of $PM_{2.5}$ in Seoul. *Chemosphere* **2020**, *251*, 126371. [CrossRef]